# ZERO-SHOT LEARNING OF CAUSAL MODELS

**Anonymous authors**
Paper under double-blind review

## ABSTRACT

With the increasing acquisition of datasets over time, we now have access to precise and varied descriptions of the world, capturing all sorts of phenomena. These datasets can be seen as empirical observations of unknown causal generative processes, which can commonly be described by Structural Causal Models (SCMs). Recovering these causal generative processes from observations poses formidable challenges, and often require to learn a specific generative model for each dataset. In this work, we propose to learn a *single* model capable of inferring in a zero-shot manner the causal generative processes of datasets. Rather than learning a specific SCM for each dataset, we enable the Fixed-Point Approach (FiP) proposed in Scetbon et al. (2024), to infer the generative SCMs conditionally on their empirical representations. More specifically, we propose to amortize the learning of a conditional version of FiP to infer generative SCMs from observations and causal structures on synthetically generated datasets. We show that our model is capable of predicting in zero-shot the true generative SCMs, and as a by-product, of (i) generating new dataset samples, and (ii) inferring intervened ones. Our experiments demonstrate that our amortized procedure achieves performances on par with SoTA methods trained specifically for each dataset on both in and out-of-distribution problems. To the best of our knowledge, this is the first time that SCMs are inferred in a zero-shot manner from observations, paving the way for a paradigmatic shift towards the assimilation of causal knowledge across datasets.

## 1 INTRODUCTION

Learning the causal generative process from observations is a fundamental problem in several scientific domains (Sachs et al., 2005; Foster et al., 2011; Xie et al., 2012), as it offers a comprehensive understanding of the data generation process, and allows for simulating the effect of controlled experiments/interventions. With a learned model of the generative process, one could even accelerate scientific discoveries by reliably predicting the effects of unseen interventions, eliminating the need for laboratory experiments (Ke et al., 2023; Zhang et al., 2024). Further, understanding the causal mechanisms behind the data generation process helps in robust representation learning as it provides a principled solution to tackle out-of-distribution (OOD) generalization (Arjovsky et al., 2019; Zhang et al., 2020; Schölkopf et al., 2021).

A popular approach for modeling causal processes is the structural causal model (SCM) framework (Peters et al., 2017) where causal mechanisms are modeled via structured functional relationships, and causal structures are given by directed acyclic graphs (DAGs). Since in several practical applications we only have access to observational data, the task of recovering the generative SCM from observations is an important problem in causality (Pearl, 2009). Solving this inverse problem is challenging as both the graph and the functional relationships modeling the causal mechanisms are unknown a priori. Several works have focused on the graph recovery problem by approximating the discrete search space of DAGs (Chickering, 2002; Peters et al., 2014; Deleu et al., 2022), or using continuous optimization objectives (Zheng et al., 2018; Lachapelle et al., 2019; Lippe et al., 2021). However, all these works focus only on the structure learning aspect and do not explicitly evaluate the learning of the functional mechanisms.

Another line of work has studied the recovery of the functional relationships from data, often under structural assumptions like known causal graphs or topological orders, using maximum likelihood estimation (MLE) independently per node (Blöbaum et al., 2022), autoregressive flows (Khemakhem et al., 2021; Geffner et al., 2022; Javaloy et al., 2023) to model causal generative pro-

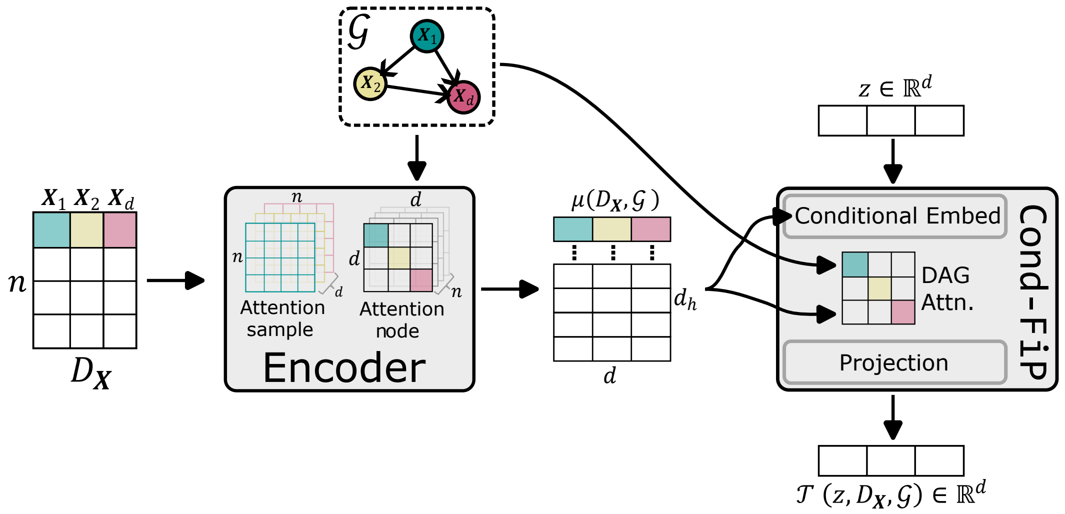

Figure 1: Sketch of the approach proposed in this work. Given a dataset of observations $D_{\boldsymbol{X}}$ and a causal graph $\boldsymbol{\mathcal{G}}$ obtained from an unkown SCM $\mathcal{S}(\mathbb{P}_{\boldsymbol{N}}, \boldsymbol{\mathcal{G}}, \boldsymbol{F})$, the encoder produces a dataset embedding $\mu(D_{\boldsymbol{X}}, \boldsymbol{\mathcal{G}})$, which serves as a condition to instantiate Cond-FiP. Then for any point $\boldsymbol{z} \in \mathbb{R}^d$, $\mathcal{T}(\boldsymbol{z}, D_{\boldsymbol{X}}, \boldsymbol{\mathcal{G}})$ aims at replicating the functional mechanism $\boldsymbol{F}(\boldsymbol{z})$ of the generative SCM.

cesses, or transformer-based architectures to model SCMs as fixed-point (FiP) problems (Scetbon et al., 2024). Despite these advances, a major limitation remains: each new dataset of observations requires training a specific model, which prevents sharing of causal knowledge across datasets.

Amortized learning (Amos, 2022) allows knowledge sharing across datasets through a supervised training objective. Rather than optimizing the parameters of a specific model for each dataset, amortized methods aim at training a *single* model that learn to predict the solutions to various instances of the same optimization problem by exploiting their shared structure. Once trained, such methods enables zero-shot inference (without updating parameters) to new problems at test time. This also connects with the recent literature on in-context learning of function classes using transformers (Garg et al., 2022; Von Oswald et al., 2023) and is a first step towards developing foundation models for causal reasoning. Recent works have proposed techniques for amortized causal structure learning (Lorch et al., 2022; Ke et al., 2022; Scetbon et al., 2024), ATE estimation (Zhang et al., 2023), and model selection for causal discovery (Gupta et al., 2023). However, none of these works have yet amortized the learning of the functional relationships to directly infer the SCMs.

**Contributions.** In this work, we introduce a conditional version of FiP (Scetbon et al., 2024), termed Cond-FiP, that zero-shot predicts the functional mechanisms of SCMs associated with datasets given their causal graphs. As a by-product, our approach can perform zero-shot generation of new dataset samples and simulation of interventions. Our contributions are summarized below.

- We propose a novel framework enabling the amortized learning of causal generative models from their empirical representations.
  - To achieve this, we first propose to amortize the learning of an encoder model that aims at inferring the noise from observational data and causal structures, and use its latent representations as embeddings of datasets.
  - Then, we introduce a conditional version of FiP (Scetbon et al., 2024), termed Cond-FiP, that leverages the latent representation of datasets obtained by our encoder and use them as conditions to infer their associated functional mechanisms.
- Given a dataset and its causal structure, our approach enables zero-shot generation of new dataset samples and simulation of intervened ones.
- We show empirically that our method achieves similar performances as the state-of-the-art approaches trained specifically for each dataset on both in and out-of-distribution problems.

### 1.1 Related Works

**Amortized Causal Learning.** Amortized methods have been explored in causality research in order to learn general algorithms that can infer in a zero-shot manner causal knowledge from observations. (Zhang et al., 2023) proposed to amortize the learning of a causal inference method to estimate average treatment effect (ATE), (Gupta et al., 2023) used amortized learning to perform model selection for causal discovery, and (Lorch et al., 2022; Ke et al., 2022; Wu et al., 2024; Scetbon et al., 2024) proposed to infer causal structures, such as causal graphs or topological orders, from observations using amortized learning. All these methods rely on the availability of synthetic datasets generated during training, enabling their learning using supervised objectives to predict the causal knowledge of interest. In this work, we extend this line of works, and propose to infer in a zero-shot manner the functional relationships of SCMs from observations and their associated causal structures. To achieve this, we propose to amortize the learning of causal embeddings of synthetically generated datasets, which then served as conditions to train a generalized version of FiP (Scetbon et al., 2024) that infers the generative SCMs in zero-shot.

**Autoregressive Causal Learning.** While a vast majority of the literature on causal discovery concerns structure learning, recent works on causal autoregressive flows (Khemakhem et al., 2021; Javaloy et al., 2023) focus on state-of-the-art generative modeling techniques for learning the causal generative processes induced by SCMs. Khemakhem et al. (2021) proved a novel connection between SCMs and autoregressive flows, as the mapping from noise variables to observable variables in SCMs is a triangular map given the topological order of the causal graph. While their work restricted the functional relationships to additive and affine flows, this was extended by Javaloy et al. (2023) to more flexible triangular monotonic increasing maps. More recently, Scetbon et al. (2024) proposed to directly model SCMs, viewed as fixed-point problems on the ordered nodes, using transformer-based architectures. While these methods enable efficient learning of SCMs and their generative processes, they all require to train a specific generative model per dataset. In contrast, we present a novel extension of FiP (Scetbon et al., 2024) by conditioning the fixed-point process on dataset embeddings, thereby amortizing the learning of functional relationships across different instances from the functional class of SCMs.

## 2 Background on Causal Learning

**Structural Causal Models.** An SCM defines the causal generative process of a set of $d$ endogenous (causal) random variables $\boldsymbol{V} = \{X_1, \cdots, X_d\}$, where each causal variable $X_i$ is defined as a function of a subset of other causal variables ($\boldsymbol{V} \setminus \{X_i\}$) and an exogenous noise variable $N_i$:

$$X_i = F_i(PA(X_i), N_i) \quad \text{s.t.} \;\; PA(X_i) \subset \boldsymbol{V} \; , \;\; X_i \notin PA(X_i) \; . \tag{1}$$

Hence, an SCM describes the data-generation process of $\boldsymbol{X} := [X_1, \cdots, X_d] \sim \mathbb{P}_{\boldsymbol{X}}$ from the noise variables $\boldsymbol{N} := [N_1, \cdots, N_d] \sim \mathbb{P}_{\boldsymbol{N}}$ via the function $\boldsymbol{F} := [F_1, \cdots, F_d]$, and a graph $\boldsymbol{\mathcal{G}} \in \{0,1\}^{d\times d}$ indicating the parents of each variable $X_i$, that is $[\boldsymbol{\mathcal{G}}]_{i,j} := 1$ if $X_j \in PA(X_i)$. $\boldsymbol{\mathcal{G}}$ is assumed to be a directed and acyclic graph (DAG), and we say the SCM is Markovian if the exogenous variable distribution $\mathbb{P}_{\boldsymbol{N}}$ has mutually independent components. In the following, we always assume SCMs to be Markovian and denote them $\mathcal{S}(\mathbb{P}_{\boldsymbol{N}}, \boldsymbol{\mathcal{G}}, \boldsymbol{F})$. In addition, we only consider additive noise models (ANM), which are SCMs of the form $X_i = F_i(PA(X_i)) + N_i$.

**DAG-Attention Mechanism.** In (Scetbon et al., 2024) the authors propose to leverage the transformer architecture to learn SCMs from observations. By reparameterizing an SCM according to a topological ordering induced by its graph, the authors show that any SCM can be reformulated as a fixed-point problem of the form $\boldsymbol{X} = \boldsymbol{H}(\boldsymbol{X}, \boldsymbol{N})$ where $\boldsymbol{H}$ admits a simple triangular structure:

$$[\text{Jac}_{\boldsymbol{x}} \boldsymbol{H}(\boldsymbol{x}, \boldsymbol{n})]_{i,j} = 0, \quad \text{if} \quad j \geq i, \quad \text{and} \quad [\text{Jac}_{\boldsymbol{n}} \boldsymbol{H}(\boldsymbol{x}, \boldsymbol{n})]_{i,j} \;\; = 0, \quad \text{if} \quad i \neq j,$$

and $\text{Jac}_{\boldsymbol{x}} \boldsymbol{H}$, $\text{Jac}_{\boldsymbol{n}} \boldsymbol{H}$ denote the Jacobian of $\boldsymbol{H}$ w.r.t the first and second variables respectively.

Motivated by this fixed-point reformulation, Scetbon et al. (2024) consider a transformed-based architecture to model the functional relationships of SCMs and propose a new attention mechanism to represent DAGs in a differentiable manner. Recall that the standard attention matrix is defined as:

$$\mathrm{A}_{\boldsymbol{M}}(\boldsymbol{Q},\boldsymbol{K}) = \frac{\exp((\boldsymbol{Q}\boldsymbol{K}^T - \boldsymbol{M})/\sqrt{d_h})}{\exp((\boldsymbol{Q}\boldsymbol{K}^T - \boldsymbol{M})/\sqrt{d_h})\ \mathbf{1}_d} \tag{2}$$

where $\boldsymbol{Q},\boldsymbol{K} \in \mathbb{R}^{d\times d_h}$ denote the keys and queries for a single attention head, and $\boldsymbol{M} \in \{0,+\infty\}^{d\times d}$ is a (potential) mask. In our setting, each row $i \in \{1,\dots,d\}$ of $\boldsymbol{Q},\boldsymbol{K}$ can be seen as a high dimensional representation (living in $\mathbb{R}^{d_h}$) of the node $i$, and when $\boldsymbol{M}$ is chosen to be a strictly lower triangular mask, the attention mechanism (2) enables to parameterize the effects of previous nodes on the current ones. However, the normalization inherent to the softmax operator in standard attention mechanisms prevents effective modeling of root nodes, which *should not* be influenced by any other node in the graph. To alleviate this issue, Scetbon et al. (2024) propose to considering the following formulation instead:

$$\mathrm{DA}_{\boldsymbol{M}}(\boldsymbol{Q},\boldsymbol{K}) = \frac{\exp((\boldsymbol{Q}\boldsymbol{K}^T - \boldsymbol{M})/\sqrt{d_h})}{\mathcal{V}\big(\ \exp((\boldsymbol{Q}\boldsymbol{K}^T - \boldsymbol{M})/\sqrt{d_h})\ \mathbf{1}_d\big)} \tag{3}$$

where $\mathcal{V}_i(\boldsymbol{v}) = v_i$ if $v_i \geq 1$, else $\mathcal{V}_i(\boldsymbol{v}) = 1$ for any $\boldsymbol{v} \in \mathbb{R}^d$. While softmax forces the coefficients along each row of the attention matrix to sum to one, the attention mechanism described in (3) allows the rows to sum in $[0,1]$, thus enabling to model root nodes in attention.

## 3 Conditional FiP

In this work, we propose to infer in zero-shot the generative SCMs from observations and causal structures using amortized training on synthetically generated problems. Our approach is composed of two key components: (1) a dataset encoder that generates dataset embeddings based on observations and causal structures, and (2) a conditional variant of FiP (Scetbon et al., 2024), designed to infer in zero-shot the generative SCMs of datasets when conditioned on their dataset embeddings produced by the encoder. In the following, we first present our dataset encoder, then introduce cond-FiP, and conclude by the use case of generating new observational and interventional samples.

### 3.1 Dataset Encoder

The objective of this section is to develop a method capable of producing efficient latent representations of datasets. To achieve this, we propose to train an encoder that predicts in zero-shot the noise samples from their associated observations given the causal structures using amortized learning. The latent representations obtained by our encoder will be used later as dataset embeddings to infer SCMs in a zero-shot manner.

**Training Setting.** We consider the amortized setting where at training time, we have access to empirical representations of $K$ SCMs $\big(\mathcal{S}(\mathbb{P}_{\boldsymbol{N}}^{(k)},\boldsymbol{\mathcal{G}}^{(k)},\boldsymbol{F}^{(k)})\big)_{k=1}^{K}$ that have been sampled independently according to a distribution of SCMs $\mathcal{S}(\mathbb{P}_{\boldsymbol{N}}^{(k)},\boldsymbol{\mathcal{G}}^{(k)},\boldsymbol{F}^{(k)}) \sim \mathbb{P}_{\mathcal{S}}$. These empirical representations, denoted $(D_{\boldsymbol{X}}^{(k)},\boldsymbol{\mathcal{G}}^{(k)})_{k=1}^{K}$ respectively, contain each $n$ observations $D_{\boldsymbol{X}}^{(k)} := [\boldsymbol{X}_1^{(k)},\dots,\boldsymbol{X}_n^{(k)}]^T \in \mathbb{R}^{n\times d}$, and the causal graph $\boldsymbol{\mathcal{G}}^{(k)} \in \{0,1\}^{d\times d}$. At training time, we also require to have access to the associated noise samples $D_{\boldsymbol{N}}^{(k)} := [\boldsymbol{N}_1^{(k)},\dots,\boldsymbol{N}_n^{(k)}]^T \in \mathbb{R}^{n\times d}$, which play the role of the target variable in our supervised task. For the sake of clarity, we will omit the dependence on $k$ in our notation and assume access to the full distribution of SCMs $\mathbb{P}_{\mathcal{S}}$. Our goal here is to learn a model that given a dataset of observations $D_{\boldsymbol{X}}$ and the causal graph associated $\boldsymbol{\mathcal{G}}$, recovers the true noise $D_{\boldsymbol{N}}$ from which the observations have been generated. By solving this prediction task, we expect the trained model to provide efficient dataset embeddings as detailed below.

**Encoder Architecture.** Following (Lorch et al., 2021; Scetbon et al., 2024), we propose to encode datasets using a transformer-based architecture that alternatively attends on both the sample and node dimensions of the input. More specifically, after having embedded the dataset $D_{\boldsymbol{X}}$ into a higher dimensional space using a linear operation $L(D_{\boldsymbol{X}}) \in \mathbb{R}^{n\times d\times d_h}$ where $d_h$ is the hidden dimension, the encoder $E$ alternates the application of transformer blocks, consisting of a self-attention block followed by an MLP block (Vaswani et al., 2017), where the attention mechanism is applied either across the samples $n$ or the nodes $d$. When attending over samples, the encoder uses standard self-attention as defined in (2) without masking ($\boldsymbol{M} = \{0\}^{n\times n}$), however, when the model attends over the nodes, we leverage the knowledge of the causal graph to mask the undesirable relationships between the nodes, that is we set $\boldsymbol{M} = +\infty \times (1 - \boldsymbol{\mathcal{G}})$, with the convention that $0 \times (+\infty) = 0$, in the standard attention (2). Finally, the obtained embeddings $E(L(D_{\boldsymbol{X}}), \boldsymbol{\mathcal{G}}) \in \mathbb{R}^{n\times d\times d_h}$ are passed to a prediction network $H : \mathbb{R}^{n\times d\times d_h} \to \mathbb{R}^{n\times d}$ defined as 2-hidden layers MLP which brings back the encoded datasets to their original space.

**Training Procedure.** To infer the noise samples in a zero-shot manner, we propose to minimize the mean squared error (MSE) of predicting the target noises $D_{\boldsymbol{N}}$ from the input $(D_{\boldsymbol{X}}, \boldsymbol{\mathcal{G}})$ over the distribution of SCMs $\mathbb{P}_{\mathcal{S}}$ available during training:

$$\mathbb{E}_{\mathcal{S}\sim\mathbb{P}_{\mathcal{S}}} ||D_{\boldsymbol{N}} - H \circ E(L(D_{\boldsymbol{X}}), \boldsymbol{\mathcal{G}})||_2^2 \; .$$

Further, as we restrict ourselves to the case of ANMs, we can equivalently reformulate our training objective in order to predict the functional relationships rather than the noise samples. Indeed, recall that for an ANM $\mathcal{S}(\mathbb{P}_{\boldsymbol{N}}, \boldsymbol{\mathcal{G}}, \boldsymbol{F})$, we have by definition that $\boldsymbol{F}(\boldsymbol{X}) = \boldsymbol{X} - \boldsymbol{N}$. Therefore, by denoting the new targets as $\boldsymbol{F}(D_{\boldsymbol{X}}) := D_{\boldsymbol{X}} - D_{\boldsymbol{N}}$, we propose instead to train our encoder to predict the evaluations of the functional relationships over the SCM distribution by minimizing:

$$\mathbb{E}_{\mathcal{S}\sim\mathbb{P}_{\mathcal{S}}} ||\boldsymbol{F}(D_{\boldsymbol{X}}) - H \circ E(L(D_{\boldsymbol{X}}), \boldsymbol{\mathcal{G}})||_2^2 \; .$$

**Inference.** Given a new dataset $D_{\boldsymbol{X}}$ and its causal graph $\boldsymbol{\mathcal{G}}$, the proposed encoder is able to both provide an embedding $E(L(D_{\boldsymbol{X}}), \boldsymbol{\mathcal{G}}) \in \mathbb{R}^{n\times d\times d_h}$, and to evaluate the functional mechanisms associated to the current observations $\widehat{F}(D_{\boldsymbol{X}}) := H \circ E(L(D_{\boldsymbol{X}}), \boldsymbol{\mathcal{G}})$. However, this model alone is insufficient for generating new data, whether observational or interventional. This task will be addressed by our conditional decoder, which is detailed in the following section.

**On the Knowledge of Graphs at Inference.** Prior works on amortized causal learning (Lorch et al., 2022; Ke et al., 2022) proposed to learn to predict the causal graphs using only observations $D_{\boldsymbol{X}}$ on synthetically generated datasets. These methods justify our setup where the true graphs are provided as part of the input context to the model, as we can use them to infer in a zero-shot manner the causal graphs from observations if the true graphs information was not available.

## 3.2 COND-FIP: CONDITIONAL FIXED-POINT DECODER

In this section, we present our proposed approach to infer the functional mechanisms of SCMs in zero-shot via amortized training using synthetically generated datasets. To do so, we propose to extend the formulation of FiP introduced in Scetbon et al. (2024) by enabling it to predict functions, and use the dataset embeddings $E(L(D_{\boldsymbol{X}}), \boldsymbol{\mathcal{G}})$ obtained by our trained encoder as conditions to infer the correct functional mechanisms of the associated SCMs. See Figure 1 for a sketch of Cond-FiP.

**Training Setting.** Analogous to the encoder training setup, we assume that we have access to a distribution of SCMs $\mathcal{S}(\mathbb{P}_{\boldsymbol{N}}, \boldsymbol{\mathcal{G}}, \boldsymbol{F}) \sim \mathbb{P}_{\mathcal{S}}$ at training time, from which we can extract empirical representations of the form $(D_{\boldsymbol{X}}, \boldsymbol{\mathcal{G}})$ containing the observations and the associated causal graphs respectively. Here, we aim at learning a *single* model $\mathcal{T}$ that can infer in zero-shot the functional mechanisms of an SCM given its empirical representation. More formally, we aim at training $\mathcal{T}$ such that for given any dataset $D_{\boldsymbol{X}}$ and its associated causal graph $\boldsymbol{\mathcal{G}}$ obtained from an SCM $\mathcal{S}(\mathbb{P}_{\boldsymbol{N}}, \boldsymbol{\mathcal{G}}, \boldsymbol{F}) \sim \mathbb{P}_{\mathcal{S}}$, the conditional function $\boldsymbol{z} \in \mathbb{R}^d \to \mathcal{T}(\boldsymbol{z}, D_{\boldsymbol{X}}, \boldsymbol{\mathcal{G}}) \in \mathbb{R}^d$ induced by the model approximates the true functional relationship $\boldsymbol{F} : \boldsymbol{z} \in \mathbb{R}^d \to \boldsymbol{F}(\boldsymbol{z}) \in \mathbb{R}^d$. We achieve this by enabling the fixed-point approach of (Scetbon et al., 2024) to be conditioned on dataset embeddings provided by our dataset encoder. We detail our procedure below.

**Decoder Architecture.** The design of our decoder is based on the FiP architecture (Scetbon et al., 2024) for fixed-point SCM learning, with two major differences enabling conditional predictions: (1) we use the dataset embeddings obtained from our encoder as a high dimensional codebook to embed the nodes, and (2) we leverage adaptive layer norm operators (Peebles & Xie, 2023) in the transformer blocks of FiP to enable conditional attention mechanisms.

**Conditional Embedding.** The key change of our decoder compared to the original FiP is in the embedding of the input. Scetbon et al. (2024) propose to embed a data point $\boldsymbol{z} := [z_1, \ldots, z_d] \in \mathbb{R}^d$ into a high dimensional space using a learnable codebook $\boldsymbol{C} := [C_1, \ldots, C_d]^T \in \mathbb{R}^{d \times d_h}$ and positional embedding $\boldsymbol{P} := [P_1, \ldots, P_d]^T \in \mathbb{R}^{d \times d_h}$, from which they define:

$$\boldsymbol{z}_{\text{emb}} := [z_1 * C_1, \ldots, z_d * C_d]^T + \boldsymbol{P} \in \mathbb{R}^{d \times d_h} .$$

By doing so, Scetbon et al. (2024) ensures that the embedded samples admit the same causal structure as the original samples. However, this embedding layer is only adapted if the samples considered are all drawn from the same observational distribution, as the representation of the nodes, that is given by the codebook $\boldsymbol{C}$, is fixed. In order to generalize their embedding strategy to the case where multiple SCMs are considered, we consider conditional codebooks and positional embeddings adapted for each dataset. More formally, given a dataset $D_{\boldsymbol{X}}$ and a causal graph $\boldsymbol{\mathcal{G}}$, we propose to define the conditional codebook and positional embedding associated as

$$\boldsymbol{C}(D_{\boldsymbol{X}}, \boldsymbol{\mathcal{G}}) := \mu(D_{\boldsymbol{X}}, \boldsymbol{\mathcal{G}}) W_{\boldsymbol{C}}, \text{ and } \boldsymbol{P}(D_{\boldsymbol{X}}, \boldsymbol{\mathcal{G}}) := \mu(D_{\boldsymbol{X}}, \boldsymbol{\mathcal{G}}) W_{\boldsymbol{P}} ,$$

where $\mu(D_{\boldsymbol{X}}, \boldsymbol{\mathcal{G}}) := \text{MaxPool}(E(L(D_{\boldsymbol{X}}), \boldsymbol{\mathcal{G}})) \in \mathbb{R}^{d \times d_h}$ is obtained by max-pooling w.r.t the sample dimension the dataset embedding $E(L(D_{\boldsymbol{X}}), \boldsymbol{\mathcal{G}}) \in \mathbb{R}^{n \times d \times d_h}$ produced by our trained encoder, and $W_{\boldsymbol{C}}, W_{\boldsymbol{P}} \in \mathbb{R}^{d_h \times d_h}$ are learnable parameters. Then we propose to embed any point $\boldsymbol{z} \in \mathbb{R}^d$ conditionally on $(D_{\boldsymbol{X}}, \boldsymbol{\mathcal{G}})$ by considering:

$$\boldsymbol{z}_{\text{emb}} := [z_1 * C_1(D_{\boldsymbol{X}}, \boldsymbol{\mathcal{G}}), \ldots, z_d * C_d(D_{\boldsymbol{X}}, \boldsymbol{\mathcal{G}})]^T + \boldsymbol{P}(D_{\boldsymbol{X}}, \boldsymbol{\mathcal{G}}) \in \mathbb{R}^{d \times d_h} .$$

**Adaptive Transfomer Block.** Once an input $\boldsymbol{z} \in \mathbb{R}^d$ has been embedded into a higher dimensional space $\boldsymbol{z}_{\text{emb}} \in \mathbb{R}^{d \times d_h}$, Scetbon et al. (2024) propose to modelize SCMs by simulating the reconstruction of the data from noise. Starting from $\boldsymbol{n}_0 \in \mathbb{R}^{d \times d_h}$ a learnable parameter, they propose to update the current noise $L \geq 1$ times by computing:

$$\boldsymbol{n}_{\ell+1} = h(\text{DA}_{\boldsymbol{M}}(\boldsymbol{n}_\ell, \boldsymbol{z}_{\text{emb}}) \boldsymbol{z}_{\text{emb}} + \boldsymbol{n}_\ell)$$

where $h$ refers to the MLP block, and for clarity, we omit both the layer's dependence on its parameters and the inclusion of layer normalization in the notation. Note that here the authors consider their DAG-Attention (3) mechanism in order to modelize correctly the root nodes of the SCM. To obtain a conditional formulation of their computational scheme, we propose first to replace the starting noise $\boldsymbol{n}_0$ by a conditional one w.r.t. $(D_{\boldsymbol{X}}, \boldsymbol{\mathcal{G}})$ and defined as $\boldsymbol{n}_0 := \mu(D_{\boldsymbol{X}}, \boldsymbol{\mathcal{G}}) W_{\boldsymbol{n}_0} \in \mathbb{R}^{d \times d_h}$, where $W_{\boldsymbol{n}_0} \in \mathbb{R}^{d_h \times d_h}$ is a learnable parameter. Additionally, we propose to add adaptive layer normalization operators (Peebles & Xie, 2023) to both attention and MLP blocks, where each scale or shift is obtained by applying a 1 hidden-layer MLP to the condition, which in our case is $\mu(D_{\boldsymbol{X}}, \boldsymbol{\mathcal{G}})$.

**Projection.** To project back the latent representation of $\boldsymbol{z}$ obtained from previous stages, that is $\boldsymbol{n}_L \in \mathbb{R}^{d \times d_h}$, we propose to simply use a linear operation to get $\widehat{\boldsymbol{z}} = \boldsymbol{n}_L W_{\text{out}} \in \mathbb{R}^d$, where $W_{\text{out}} \in \mathbb{R}^{d_h}$ is learnable. In the following, we denote the overall architecture $\mathcal{T}$, which given an input $\boldsymbol{z} \in \mathbb{R}^d$ and some condition $(D_{\boldsymbol{X}}, \boldsymbol{\mathcal{G}})$ outputs $\widehat{\boldsymbol{z}}$, that is $\mathcal{T}(\boldsymbol{z}, D_{\boldsymbol{X}}, \boldsymbol{\mathcal{G}}) = \widehat{\boldsymbol{z}}$. Note that, for simplicity, we omit the dependence of $\widehat{\boldsymbol{z}}$ on $(D_{\boldsymbol{X}}, \boldsymbol{\mathcal{G}})$ in the notation.

**Training Procedure.** Recall that our goal is infer in zero-shot the functional mechanisms of SCMs given their empirical representations. Therefore, to train our model $\mathcal{T}$, we propose to minimize the reconstruction error of the true functional mechanisms estimated by our model over the distribution of SCMs $\mathbb{P}_{\mathcal{S}}$. More precisely, for any SCM $\mathcal{S}(\mathbb{P}_{\boldsymbol{N}}, \boldsymbol{\mathcal{G}}, \boldsymbol{F}) \sim \mathbb{P}_{\mathcal{S}}$ and its empirical representation $(D_{\boldsymbol{X}}, \boldsymbol{\mathcal{G}})$, we aim at minimizing

$$\mathbb{E}_{\boldsymbol{z} \sim \mathbb{P}_{\boldsymbol{X}}} \|\mathcal{T}(\boldsymbol{z}, D_{\boldsymbol{X}}, \boldsymbol{\mathcal{G}}) - \boldsymbol{F}(\boldsymbol{z})\|_2^2 \tag{4}$$

where $\boldsymbol{z} \sim \mathbb{P}_{\boldsymbol{X}}$ is chosen independent of the random dataset $D_{\boldsymbol{X}}$. Therefore, when integrating over the distribution of SCMs, we obtain the following optimization problem:

$$\mathbb{E}_{\mathcal{S} \sim \mathbb{P}_{\mathcal{S}}} \mathbb{E}_{\boldsymbol{z} \sim \mathbb{P}_{\boldsymbol{X}}} \|\mathcal{T}(\boldsymbol{z}, D_{\boldsymbol{X}}, \boldsymbol{\mathcal{G}}) - \boldsymbol{F}(\boldsymbol{z})\|_2^2 .$$

To compute (4), we propose to sample $n$ independent samples $\boldsymbol{X}_1', \ldots, \boldsymbol{X}_n'$ from $\mathbb{P}_{\boldsymbol{X}}$, leading to a new dataset $D_{\boldsymbol{X}'}$ independent of $D_{\boldsymbol{X}}$, from which we obtain the following optimization problem:

$$\mathbb{E}_{\mathcal{S} \sim \mathbb{P}_{\mathcal{S}}} \|\mathcal{T}(D_{\boldsymbol{X}'}, D_{\boldsymbol{X}}, \boldsymbol{\mathcal{G}}) - \boldsymbol{F}(D_{\boldsymbol{X}'})\|_2^2 .$$

Therefore our training objective aims at learning $\mathcal{T}$ such that for any given empirical representation $(D_{\boldsymbol{X}}, \boldsymbol{\mathcal{G}})$ of an unknown SCM $\mathcal{S}(\mathbb{P}_{\boldsymbol{N}}, \boldsymbol{\mathcal{G}}, \boldsymbol{F}) \sim \mathbb{P}_{\mathcal{S}}$, the conditional function induced by our model, that is $\boldsymbol{z} \to \mathcal{T}(\boldsymbol{z}, D_{\boldsymbol{X}}, \boldsymbol{\mathcal{G}})$, is close to the true functional mechanism $\boldsymbol{F}$ in the MSE sense. In the following, we explain in more detail how to use cond-FiP for causal generation and inference tasks.

### 3.3 Inference with Cond-FiP: Generation and Intervention

**Generation with Cond-FiP.** Cond-FiP is capable of generating new data samples: given a random vector noise $\boldsymbol{n} \sim \mathbb{P}_{\boldsymbol{N}}$, we can estimate the observational sample associated according to an unknown SCM $\mathcal{S}(\mathbb{P}_{\boldsymbol{N}}, \boldsymbol{\mathcal{G}}, \boldsymbol{F}) \sim \mathbb{P}_{\mathcal{S}}$ as long as we have access to its empirical representation $(D_{\boldsymbol{X}}, \boldsymbol{\mathcal{G}})$. More formally, starting from $\boldsymbol{n}_0 = \boldsymbol{n}$, we infer the associated observation by computing for $\ell = 1, \dots, d$:

$$\boldsymbol{n}_\ell = \mathcal{T}(\boldsymbol{n}_{\ell-1}, D_{\boldsymbol{X}}, \boldsymbol{\mathcal{G}}) + \boldsymbol{n}\ . \tag{5}$$

After (at most) $d$ iterations, $\boldsymbol{n}_d$ corresponds to the observational sample associated to the original noise $\boldsymbol{n}$ according to our conditional SCM $\mathcal{T}(\cdot, D_{\boldsymbol{X}}, \boldsymbol{\mathcal{G}})$. To sample noise from $\mathbb{P}_{\boldsymbol{N}}$, we leverage cond-FiP that can estimates noise samples under the ANM assumption by computing $\widehat{D_{\boldsymbol{N}}} := D_{\boldsymbol{X}} - \mathcal{T}(D_{\boldsymbol{X}}, E(L(D_{\boldsymbol{X}}), \boldsymbol{\mathcal{G}})$. From these estimated noise samples, we can efficiently estimate the joint distribution of the noise thanks to the Markovian assumption by computing the inverse cdfs of the marginals as proposed in Scetbon et al. (2024).

**Interventional Predictions.** Cond-FiP also enables the estimation of interventions given an empirical representation $(D_{\boldsymbol{X}}, \boldsymbol{\mathcal{G}})$ of an unkown SCM $\mathcal{S}(\mathbb{P}_{\boldsymbol{N}}, \boldsymbol{\mathcal{G}}, \boldsymbol{F}) \sim \mathbb{P}_{\mathcal{S}}$. To achieve this, we start from a noise sample $\boldsymbol{n}$, and we generate the associated intervened sample $\widehat{\boldsymbol{z}}^{\text{do}}$ by directly modifying the conditional SCM provided by Cond-FiP. More specifically, we modify in place the SCM obtained by Cond-FiP, leading to its interventional version $\mathcal{T}^{\text{do}}(\cdot, D_{\boldsymbol{X}}, \boldsymbol{\mathcal{G}})$. Now, generating an intervened sample can be done by applying the loop defined in (5), starting from $\boldsymbol{n}$ and using the intervened SCM $\mathcal{T}^{\text{do}}(\cdot, D_{\boldsymbol{X}}, \boldsymbol{\mathcal{G}})$ rather than the original one.

## 4 Experiments

We begin by describing our experimental setup in Section 4.1, where we detail the training and inference procedures for Cond-FiP, along with the model configurations. Then, we present the results of our empirical analysis, comparing Cond-FiP with other state-of-the-art baselines in Section 4.2.

### 4.1 Experimental Setup

**Data Generation Process.** We use the synthetic data generation procedure proposed by Lorch et al. (2022) to generate SCMs in our empirical study, as it offers a wide variety of SCMs, making it ideal for amortized training. We have the option to sample graphs as per the following schemes: Erods-Renyi (Erdos & Renyi, 1959), scale-free models (Barabási & Albert, 1999), Watts-Strogatz (Watts & Strogatz, 1998), and stochastic block models (Holland et al., 1983). To sample noise variables, we can choose from either the gaussian or laplace distribution where variances are sampled randomly. Further, we can control the complexity of causal relationships: either we set them to be linear (LIN) functions randomly sampled, or use random fourier features (RFF) for generating random non-linear causal relationships. We construct two distribution of SCMs $\mathbb{P}_{\text{IN}}$, and $\mathbb{P}_{\text{OUT}}$, which vary based on the choice for sampling causal graphs, noise variables, and causal relationships. The classification aids in understanding the creation of train and test datasets.

- **In Distribution ($\mathbb{P}_{\text{IN}}$):** We sample causal graphs using the Erods-Renyi and scale-free models schemes. Noise variables are sampled from the gaussian distribution, and we allow for both LIN and RFF causal relationships.
- **Out of Distribution ($\mathbb{P}_{\text{OUT}}$):** Causal graphs are drawn from Watts-Strogatz and stochastic block models schemes. Noise variables follow the laplace distribution, and both the LIN and RFF cases are used to sample functions. However, the parameters of these distributions are sampled from a different range as compared to $\mathbb{P}_{\text{IN}}$ to create a distribution shift.

**Training Datasets.** We randomly sample SCMs from the $\mathbb{P}_{\text{IN}}$ distribution, and we restrict the total nodes of each SCM to be $d = 20$ nodes. From each of these SCMs, we extract the causal graph $\boldsymbol{\mathcal{G}}$ and further generate $n_{\text{train}} = 400$ observations to obtain $D_{\boldsymbol{X}}$. This procedure is used for generating the training datasets for both amortized training of the dataset encoder and Cond-FiP. In total, we generate $\simeq 4e6$ SCMs to train our models.

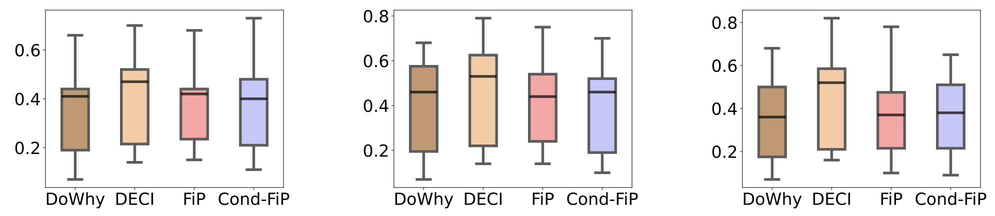

(a) Noise Prediction (b) Sample Generation (c) Interventional Generation

Figure 2: We compare Cond-FiP against the baselines for the different evaluation tasks on the **CSuite benchmark**. The y-axis denotes the RMSE for the respective tasks across the 9 datasets.

**Test Datasets.** We evaluate the model for both in-distribution and out-of-distribution generalization by sampling datasets from $\mathbb{P}_{\text{IN}}$ and $\mathbb{P}_{\text{OUT}}$ respectively. We split our collection of test datasets into the four following categories.

- LIN **IN**: SCMs sampled from $\mathbb{P}_{\text{IN}}$ with linear functional relationships.
- RFF **IN**: SCMs sampled from $\mathbb{P}_{\text{IN}}$ with non-linear functional relationships.
- LIN **OUT**: SCMs sampled from $\mathbb{P}_{\text{OUT}}$ with linear functional relationships.
- RFF **OUT**: SCMs sampled from $\mathbb{P}_{\text{OUT}}$ with non-linear functional relationships.

For each category, we vary total nodes $d \in [10, 20, 50, 100]$ and sample for each dimension $d$ either 6 or 9 SCMs, depending on the number of possible schemes for sampling the causal graphs, from which we generate $n_{\text{test}} = 800$ observational samples. Hence, we have a total of 120 test datasets, allowing for a comprehensive evaluation of methods. An interesting aspect of our test setup is that we evaluate the model's ability to generalize to larger graphs ($d = 50$, $d = 100$) despite the train datasets containing only graphs with $d = 20$ nodes.

Further, we generate test datasets using a different synthetic data simulator, C-Suite (Geffner et al., 2022), which consists of 9 different configurations for sampling SCMs.

**Model and Training Configuration.** For both the dataset encoder and cond-FiP, we set the embedding dimension to $d_h = 256$ and the hidden dimension of MLP blocks to 512. Both of our transformer-based models contains 4 attention layers and each attention consists of 8 attention heads. The models were trained for a total of $10k$ epochs with the Adam optimizer (Paszke et al., 2017), where we used a learning rate of $1e-4$ and a weight decay of $5e-9$. We also use the EMA implementation of (Karras et al., 2023) to train our models. Each epoch contains $\simeq 400$ randomly generated datasets from the distribution $\mathbb{P}_{\text{IN}}$, which are processed with a batch size of 2 on a single L40 GPU with 48GB memory.

## 4.2 Benchmark of Cond-FiP

**Baselines.** We compare Cond-FiP against FiP (Scetbon et al., 2024), DECI (Geffner et al., 2022), and DoWhy (Blöbaum et al., 2022). We evaluate the zero-shot generalization capabilities of our amortized approach when compared to non-amortized baselines trained from scratch on each test problem instance (or dataset). For a fair comparison with our method, we use $n_{\text{train}} = 400$ samples to train baselines, and evaluate the performance on the remaining 400 test samples. Also, we provide the true graph $\mathcal{G}$ to all the baselines for consistency as Cond-FiP requires true graphs. Finally, we use 400 sample to obtain the dataset embedding, and evaluate Cond-FiP on the remaining ones.

**Evaluation Tasks.** We evaluate the performance of all the methods on the following three tasks. **Noise Prediction:** given the observations $D_{\boldsymbol{X}}$ and the true graph $\mathcal{G}$, infer the noise variables $\widehat{D_{\boldsymbol{N}}}$ and compute the root-mean-square error (RMSE) with true noise $D_{\boldsymbol{N}}$. **Sample Generation:** given the noise samples $D_{\boldsymbol{N}}$ and the true graph $\mathcal{G}$, generate the causal variables $\widehat{D_{\boldsymbol{X}}}$ and compute the RMSE with the true causal variables $D_{\boldsymbol{X}}$. **Interventional Generation:** given the noise samples $D_{\boldsymbol{N}}$ and the true graph $\mathcal{G}$, generate the intervened samples and compute the RMSE with the true intervened samples.

| Method | Total Nodes | LIN **IN** | RFF **IN** | LIN **OUT** | RFF **OUT** |
|---|---|---|---|---|---|
| `DoWhy` | 10 | 0.03 (0.0) | 0.13 (0.02) | 0.04 (0.01) | 0.11 (0.01) |
| `DECI` | 10 | 0.09 (0.01) | 0.23 (0.03) | 0.12 (0.01) | 0.23 (0.03) |
| `FiP` | 10 | 0.04 (0.0) | 0.09 (0.01) | 0.06 (0.01) | 0.08 (0.01) |
| `Cond-FiP` | 10 | 0.06 (0.01) | 0.1 (0.01) | 0.07 (0.01) | 0.1 (0.01) |
| `DoWhy` | 20 | 0.03 (0.01) | 0.15 (0.02) | 0.03 (0.0) | 0.23 (0.01) |
| `DECI` | 20 | 0.10 (0.02) | 0.21 (0.03) | 0.08 (0.02) | 0.23 (0.02) |
| `FiP` | 20 | 0.04 (0.0) | 0.12 (0.02) | 0.05 (0.0) | 0.15 (0.02) |
| `Cond-FiP` | 20 | 0.06 (0.01) | 0.09 (0.01) | 0.07 (0.0) | 0.12 (0.0) |
| `DoWhy` | 50 | 0.03 (0.0) | 0.18 (0.03) | 0.03 (0.0) | 0.29 (0.03) |
| `DECI` | 50 | 0.09 (0.01) | 0.24 (0.02) | 0.07 (0.01) | 0.29 (0.02) |
| `FiP` | 50 | 0.04 (0.0) | 0.14 (0.03) | 0.04 (0.0) | 0.23 (0.04) |
| `Cond-FiP` | 50 | 0.06 (0.01) | 0.10 (0.01) | 0.07 (0.01) | 0.14 (0.01) |
| `DoWhy` | 100 | 0.03 (0.0) | 0.2 (0.03) | 0.03 (0.0) | 0.31 (0.02) |
| `DECI` | 100 | 0.08 (0.02) | 0.26 (0.03) | 0.07 (0.01) | 0.30 (0.02) |
| `FiP` | 100 | 0.04 (0.0) | 0.16 (0.03) | 0.04 (0.0) | 0.24 (0.02) |
| `Cond-FiP` | 100 | 0.05 (0.0) | 0.1 (0.01) | 0.07 (0.01) | 0.16 (0.01) |

Table 1: **Results for Noise Prediction.** We compare Cond-FiP against the baselines for the task of predicting noise variables from the input observations. Each cell reports the mean (standard error) RMSE over the multiple test datasets for each scenario. Shaded rows denote the case where the graph size is larger than the train graph sizes ($d = 20$) for Cond-FiP.

**Metric.** Let us denote a predicted target as $\widehat{\boldsymbol{Y}} \in \mathbb{R}^{n_{\text{test}} \times d}$ and the true target as $\boldsymbol{Y} \in \mathbb{R}^{n_{\text{test}} \times d}$. The RMSE is computed on a sample basis and then averaged over all the test samples available. More formally, the metric used here is $\frac{1}{n_{\text{test}}} \sum_{i=1}^{n_{\text{test}}} \sqrt{\frac{1}{d} \|[\boldsymbol{Y}]_i - [\widehat{\boldsymbol{Y}}]_i\|_2^2}$. This metric allows us to compare results across different graph sizes as it is scaled by the dimension $d$.

**Results on Noise Predictions.** Table 1 presents the results for the case of inferring noise from observations. Across all the different in-distribution and out-of-distribution scenarios, Cond-FiP is competitive with the baselines that were trained from scratch at test time. Further, Cond-FiP is able to generalize to larger graphs ($d = 50, d = 100$) despite being trained for only graphs of size $d = 20$. We also obtain similar findings with the CSuite benchmark (Figure 2a), which is a different simulator than what we used for training Cond-FiP.

**Results on Sample Generation.** We now test the generative capabilities of Cond-FiP, where the models are provided with input noise variables. Table 2 presents results for generating observational data, and shows that Cond-FiP is competitive with the baselines across all the scenarios. Similar to the case of noise prediction, Cond-FiP can generalize to larger graphs at test time and is robust to datasets generated from different simulators like CSuite (Figure 2b). We also add a real-world experiment in Appendix A where we compare the distribution generated by models with the true distribution of data according to the Maximum Mean Discrepency (Gretton et al., 2012). Further, Appendix B provides results for ablations of the decoder to better understand the strategy of training with both linear and rff data.

**Results on Interventional Generation.** Cond-FiP can also simulate interventional data while being robust to distribution shifts, graph sizes (Table 3), and different simulators (Figure 2c). This is especially interesting as we never explicitly trained Cond-FiP for interventional tasks. This provide further evidence towards Cond-FiP capturing the true functional mechanisms.

**Limitations.** While Cond-FiP generalizes to new instance problems with larger graphs, it is still unable to improve its performances when given larger context sizes at inference (see Appendix C). To further enhance the generalization capabilities of our approach, we would need to scale both the model and the training data, allowing the model to encounter more complex and diverse contexts. We leave this investigation for future work.

**Conclusion** In this work, we demonstrate that a *single* model can be trained to infer Structural Causal Models (SCMs) in a zero-shot manner through amortized training. Our proposed method, Cond-FiP, not only generalizes effectively to novel SCMs at test time but also remains robust across

| Method | Total Nodes | LIN **IN** | RFF **IN** | LIN **OUT** | RFF **OUT** |
|---|---|---|---|---|---|
| `DoWhy` | 10 | 0.05 (0.0) | 0.18 (0.03) | 0.06 (0.01) | 0.12 (0.02) |
| `DECI` | 10 | 0.15 (0.02) | 0.33 (0.04) | 0.16 (0.02) | 0.27 (0.03) |
| `FiP` | 10 | 0.07 (0.0) | 0.13 (0.02) | 0.08 (0.01) | 0.11 (0.02) |
| `Cond-FiP` | 10 | 0.06 (0.01) | 0.14 (0.02) | 0.05 (0.01) | 0.08 (0.01) |
| `DoWhy` | 20 | 0.06 (0.01) | 0.27 (0.05) | 0.05 (0.0) | 0.39 (0.04) |
| `DECI` | 20 | 0.16 (0.02) | 0.39 (0.05) | 0.13 (0.02) | 0.44 (0.04) |
| `FiP` | 20 | 0.08 (0.01) | 0.23 (0.05) | 0.08 (0.01) | 0.27 (0.04) |
| `Cond-FiP` | 20 | 0.05 (0.01) | 0.24 (0.06) | 0.07 (0.01) | 0.30 (0.03) |
| `DoWhy` | 50 | 0.08 (0.01) | 0.35 (0.09) | 0.06 (0.01) | 0.54 (0.06) |
| `DECI` | 50 | 0.15 (0.01) | 0.46 (0.06) | 0.13 (0.02) | 0.67 (0.06) |
| `FiP` | 50 | 0.09 (0.01) | 0.26 (0.05) | 0.08 (0.01) | 0.48 (0.06) |
| `Cond-FiP` | 50 | 0.08 (0.01) | 0.25 (0.05) | 0.07 (0.0) | 0.48 (0.07) |
| `DoWhy` | 100 | 0.06 (0.0) | 0.33 (0.07) | 0.06 (0.01) | 0.63 (0.07) |
| `DECI` | 100 | 0.14 (0.02) | 0.50 (0.09) | 0.14 (0.02) | 0.71 (0.08) |
| `FiP` | 100 | 0.08 (0.01) | 0.3 (0.06) | 0.09 (0.01) | 0.55 (0.08) |
| `Cond-FiP` | 100 | 0.07 (0.01) | 0.29 (0.07) | 0.09 (0.01) | 0.57 (0.07) |

Table 2: **Results for Sample Generation.** We compare Cond-FiP against the baselines for the task of generating samples from the input noise variables. Each cell reports the mean (standard error) RMSE over the multiple test datasets for each scenario. Shaded rows denote the case where the graph size is larger than the train graph sizes ($d = 20$) for Cond-FiP.

| Method | Total Nodes | LIN **IN** | RFF **IN** | LIN **OUT** | RFF **OUT** |
|---|---|---|---|---|---|
| `DoWhy` | 10 | 0.08 (0.03) | 0.19 (0.04) | 0.05 (0.01) | 0.12 (0.02) |
| `DECI` | 10 | 0.17 (0.02) | 0.34 (0.04) | 0.13 (0.02) | 0.25 (0.03) |
| `FiP` | 10 | 0.08 (0.01) | 0.15 (0.02) | 0.07 (0.01) | 0.09 (0.01) |
| `Cond-FiP` | 10 | 0.10 (0.03) | 0.21 (0.03) | 0.07 (0.01) | 0.11 (0.01) |
| `DoWhy` | 20 | 0.06 (0.01) | 0.27 (0.06) | 0.05 (0.0) | 0.36 (0.03) |
| `DECI` | 20 | 0.16 (0.02) | 0.38 (0.05) | 0.15 (0.04) | 0.42 (0.03) |
| `FiP` | 20 | 0.09 (0.01) | 0.23 (0.05) | 0.12 (0.04) | 0.25 (0.03) |
| `Cond-FiP` | 20 | 0.09 (0.01) | 0.24 (0.05) | 0.14 (0.03) | 0.31 (0.03) |
| `DoWhy` | 50 | 0.08 (0.01) | 0.29 (0.05) | 0.06 (0.01) | 0.53 (0.06) |
| `DECI` | 50 | 0.17 (0.02) | 0.44 (0.06) | 0.13 (0.02) | 0.64 (0.06) |
| `FiP` | 50 | 0.11 (0.02) | 0.25 (0.05) | 0.09 (0.01) | 0.46 (0.06) |
| `Cond-FiP` | 50 | 0.13 (0.02) | 0.27 (0.04) | 0.12 (0.02) | 0.48 (0.07) |
| `DoWhy` | 100 | 0.05 (0.0) | 0.33 (0.07) | 0.06 (0.01) | 0.60 (0.07) |
| `DECI` | 100 | 0.14 (0.02) | 0.49 (0.08) | 0.15 (0.02) | 0.70 (0.08) |
| `FiP` | 100 | 0.08 (0.01) | 0.29 (0.07) | 0.10 (0.01) | 0.54 (0.08) |
| `Cond-FiP` | 100 | 0.10 (0.01) | 0.30 (0.06) | 0.14 (0.02) | 0.58 (0.07) |

Table 3: **Results for Interventional Generation.** We compare Cond-FiP against the baselines for the task of generating interventional data from the input noise variables. Each cell reports the mean (standard error) RMSE over the multiple test datasets for each scenario. Shaded rows denote the case where the graph size is larger than the train graph sizes ($d = 20$) for Cond-FiP.

varying SCM distributions. To the best of our knowledge, this is the first approach to establish the feasibility of learning causal generative models in a foundational manner. Future work will focus on scaling to larger problem instances and applying the method to real-world scenarios.

## References

Brandon Amos. Tutorial on amortized optimization for learning to optimize over continuous domains. *arXiv e-prints*, pp. arXiv–2202, 2022.

Martin Arjovsky, Léon Bottou, Ishaan Gulrajani, and David Lopez-Paz. Invariant risk minimization. *arXiv preprint arXiv:1907.02893*, 2019.

Albert-László Barabási and Réka Albert. Emergence of scaling in random networks. *science*, 286 (5439):509–512, 1999.

Patrick Blöbaum, Peter Götz, Kailash Budhathoki, Atalanti A. Mastakouri, and Dominik Janzing. Dowhy-gcm: An extension of dowhy for causal inference in graphical causal models. *arXiv preprint arXiv:2206.06821*, 2022.

David Maxwell Chickering. Optimal structure identification with greedy search. *Journal of machine learning research*, 3(Nov):507–554, 2002.

Tristan Deleu, António Góis, Chris Emezue, Mansi Rankawat, Simon Lacoste-Julien, Stefan Bauer, and Yoshua Bengio. Bayesian structure learning with generative flow networks. *arXiv preprint arXiv:2202.13903*, 2022.

P Erdos and A Renyi. On random graphs i. *Publ. math. debrecen*, 6(290-297):18, 1959.

Jared C Foster, Jeremy MG Taylor, and Stephen J Ruberg. Subgroup identification from randomized clinical trial data. *Statistics in medicine*, 30(24):2867–2880, 2011.

Shivam Garg, Dimitris Tsipras, Percy S Liang, and Gregory Valiant. What can transformers learn in-context? a case study of simple function classes. *Advances in Neural Information Processing Systems*, 35:30583–30598, 2022.

Tomas Geffner, Javier Antoran, Adam Foster, Wenbo Gong, Chao Ma, Emre Kiciman, Amit Sharma, Angus Lamb, Martin Kukla, Nick Pawlowski, et al. Deep end-to-end causal inference. *arXiv preprint arXiv:2202.02195*, 2022.

Arthur Gretton, Karsten M Borgwardt, Malte J Rasch, Bernhard Schölkopf, and Alexander Smola. A kernel two-sample test. *The Journal of Machine Learning Research*, 13(1):723–773, 2012.

Shantanu Gupta, Cheng Zhang, and Agrin Hilmkil. Learned causal method prediction. *arXiv preprint arXiv:2311.03989*, 2023.

Paul W Holland, Kathryn Blackmond Laskey, and Samuel Leinhardt. Stochastic blockmodels: First steps. *Social networks*, 5(2):109–137, 1983.

Adrián Javaloy, Pablo Sanchez-Martin, and Isabel Valera. Causal normalizing flows: from theory to practice. In *Advances in Neural Information Processing Systems*, volume 36, 2023.

Tero Karras, Miika Aittala, Jaakko Lehtinen, Janne Hellsten, Timo Aila, and Samuli Laine. Analyzing and improving the training dynamics of diffusion models. *ArXiv*, abs/2312.02696, 2023. URL `https://api.semanticscholar.org/CorpusID:265659032`.

Nan Rosemary Ke, Silvia Chiappa, Jane Wang, Anirudh Goyal, Jorg Bornschein, Melanie Rey, Theophane Weber, Matthew Botvinic, Michael Mozer, and Danilo Jimenez Rezende. Learning to induce causal structure. *arXiv preprint arXiv:2204.04875*, 2022.

Nan Rosemary Ke, Sara-Jane Dunn, Jorg Bornschein, Silvia Chiappa, Melanie Rey, Jean-Baptiste Lespiau, Albin Cassirer, Jane Wang, Theophane Weber, David Barrett, Matthew Botvinick, Anirudh Goyal, Mike Mozer, and Danilo Rezende. Discogen: Learning to discover gene regulatory networks, 2023.

Ilyes Khemakhem, Ricardo Monti, Robert Leech, and Aapo Hyvarinen. Causal autoregressive flows. In *International Conference on Artificial Intelligence and Statistics*, pp. 3520–3528. PMLR, 2021.

Sébastien Lachapelle, Philippe Brouillard, Tristan Deleu, and Simon Lacoste-Julien. Gradient-based neural dag learning. *arXiv preprint arXiv:1906.02226*, 2019.

Phillip Lippe, Taco Cohen, and Efstratios Gavves. Efficient neural causal discovery without acyclicity constraints. *arXiv preprint arXiv:2107.10483*, 2021.

Lars Lorch, Jonas Rothfuss, Bernhard Schölkopf, and Andreas Krause. Dibs: Differentiable bayesian structure learning. *Advances in Neural Information Processing Systems*, 34:24111–24123, 2021.

Lars Lorch, Scott Sussex, Jonas Rothfuss, Andreas Krause, and Bernhard Schölkopf. Amortized inference for causal structure learning. *Advances in Neural Information Processing Systems*, 35: 13104–13118, 2022.

Adam Paszke, Sam Gross, Soumith Chintala, Gregory Chanan, Edward Yang, Zachary DeVito, Zeming Lin, Alban Desmaison, Luca Antiga, and Adam Lerer. Automatic differentiation in pytorch. 2017.

Judea Pearl. *Causality*. Cambridge university press, 2009.

William Peebles and Saining Xie. Scalable diffusion models with transformers. In *Proceedings of the IEEE/CVF International Conference on Computer Vision*, pp. 4195–4205, 2023.

Jonas Peters, Joris M Mooij, Dominik Janzing, and Bernhard Schölkopf. Causal discovery with continuous additive noise models. *Journal of Machine Learning Research*, 2014.

Jonas Peters, Dominik Janzing, and Bernhard Schölkopf. *Elements of causal inference: foundations and learning algorithms*. The MIT Press, 2017.

Karen Sachs, Omar Perez, Dana Pe'er, Douglas A Lauffenburger, and Garry P Nolan. Causal protein-signaling networks derived from multiparameter single-cell data. *Science*, 308(5721): 523–529, 2005.

Meyer Scetbon, Joel Jennings, Agrin Hilmkil, Cheng Zhang, and Chao Ma. Fip: a fixed-point approach for causal generative modeling, 2024.

Bernhard Schölkopf, Francesco Locatello, Stefan Bauer, Nan Rosemary Ke, Nal Kalchbrenner, Anirudh Goyal, and Yoshua Bengio. Toward causal representation learning. *Proceedings of the IEEE*, 109(5):612–634, 2021.

Ashish Vaswani, Noam Shazeer, Niki Parmar, Jakob Uszkoreit, Llion Jones, Aidan N Gomez, Łukasz Kaiser, and Illia Polosukhin. Attention is all you need. *Advances in neural information processing systems*, 30, 2017.

Johannes Von Oswald, Eyvind Niklasson, Ettore Randazzo, João Sacramento, Alexander Mordvintsev, Andrey Zhmoginov, and Max Vladymyrov. Transformers learn in-context by gradient descent. In *International Conference on Machine Learning*, pp. 35151–35174. PMLR, 2023.

Duncan J Watts and Steven H Strogatz. Collective dynamics of 'small-world'networks. *nature*, 393 (6684):440–442, 1998.

Menghua Wu, Yujia Bao, Regina Barzilay, and Tommi Jaakkola. Sample, estimate, aggregate: A recipe for causal discovery foundation models. *arXiv preprint arXiv:2402.01929*, 2024.

Yu Xie, Jennie E Brand, and Ben Jann. Estimating heterogeneous treatment effects with observational data. *Sociological methodology*, 42(1):314–347, 2012.

Cheng Zhang, Kun Zhang, and Yingzhen Li. A causal view on robustness of neural networks. *Advances in Neural Information Processing Systems*, 33:289–301, 2020.

Jiaqi Zhang, Joel Jennings, Cheng Zhang, and Chao Ma. Towards causal foundation model: on duality between causal inference and attention. *arXiv preprint arXiv:2310.00809*, 2023.

Jiaqi Zhang, Kristjan Greenewald, Chandler Squires, Akash Srivastava, Karthikeyan Shanmugam, and Caroline Uhler. Identifiability guarantees for causal disentanglement from soft interventions. *Advances in Neural Information Processing Systems*, 36, 2024.

Xun Zheng, Bryon Aragam, Pradeep K Ravikumar, and Eric P Xing. Dags with no tears: Continuous optimization for structure learning. In S. Bengio, H. Wallach, H. Larochelle, K. Grauman, N. Cesa-Bianchi, and R. Garnett (eds.), *Advances in Neural Information Processing Systems*, volume 31. Curran Associates, Inc., 2018. URL `https://proceedings.neurips.cc/paper/2018/file/e347c51419ffb23ca3fd5050202f9c3d-Paper.pdf`.

## A Experiments on Real World Benchmark

We use the real world flow cytometry dataset (Sachs et al., 2005) to benchmark Cond-FiP againts the baselines. This dataset contains $n \simeq 800$ observational samples expressed in a $d = 11$ dimensional space, and the reference (true) causal graph. We sample a train dataset $D_{\boldsymbol{X}}^{\text{train}} \in \mathbb{R}^{n_{\text{train}} \times d}$ and test dataset $D_{\boldsymbol{X}}^{\text{test}} \in \mathbb{R}^{n_{\text{test}} \times d}$ of size $n_{\text{train}} = n_{\text{test}} = 400$ each, where the train dataset is to used to train the baselines and obtain dataset embedding for Cond-FiP.

Since we don't have access to the true functional relationships, we cannot compute RMSE for noise prediction or sample generation like we did in our experiments with synthetic benchmarks. Instead for each method, we obtain the noise predictions $\widehat{D_{\boldsymbol{N}}^{\text{train}}}$ on the train split, and use it to fit a gaussian distribution for each component (node). Then we use the learned gaussian distribution to sample new noise variables, $\widehat{D_{\boldsymbol{N}}^{\text{sample}}}$, which are mapped to the observations as per the causal mechanisms learned by each method, $\widehat{D_{\boldsymbol{X}}^{\text{sample}}}$. Finally, we compute the maximum mean discrepancy (MMD) distance between $\widehat{D_{\boldsymbol{X}}^{\text{sample}}}$ and $D_{\boldsymbol{X}}^{\text{test}}$ as metric to determine whether the method has captured the true causal relationships. For consistency, we also evaluate the reconstruction performances of the models by using directly the inferred noise $\widehat{D_{\boldsymbol{N}}^{\text{train}}}$ from the models, and the compute MMD between the reconstructed data and the test data.

Table 4 presents our results, where for reference we also report the MMD distance between the true train and test split, which should be very small since both the datasets are sampled from the same distribution. We find that Cond-FiP is competitive with the baselines that were trained from scratch. Except DoWhy, the MMD distance with reconstructed samples from the methods are close to oracle performance.

| Method | MMD($\widehat{D_{\boldsymbol{X}}^{\text{sample}}}$, $D_{\boldsymbol{X}}^{\text{test}}$) | MMD($\widehat{D_{\boldsymbol{X}}^{\text{train}}}$, $D_{\boldsymbol{X}}^{\text{test}}$) | MMD($D_{\boldsymbol{X}}^{\text{train}}$, $D_{\boldsymbol{X}}^{\text{test}}$) |
|---|---|---|---|
| `DoWhy` | 0.015 | 0.014 | 0.005 |
| `DECI` | 0.014 | 0.005 | 0.005 |
| `FiP` | 0.015 | 0.005 | 0.005 |
| `Cond-FiP` | 0.013 | 0.005 | 0.005 |

Table 4: **Results for Sachs dataset.** We compare Cond-FiP against the baselines for the task of generating sample data on the real world benchmark. Each cell reports the MMD, and we also report the reconstruction error for all of the methods.

## B Decoder Ablation Study

We conduct an ablation study where we train two variants of the decoder Cond-FiP described as follows:

- *Cond-FiP (LIN):* We sample SCMs with linear functional relationships during training.
- *Cond-FiP (RFF):* We sample SCMs with non-linear functional relationships for training.

Note that in the main results (Tabel 2, Table 3) we show the performances of Cond-FiP trained by sampling SCMs with both linear and non-linear functional relationships. Hence, this ablations helps us to understand whether the strategy of training on mixed functional relationships can bring more generalization to the amortization process, or if we should have trained decoders specialized for linear and non-linear functional relationships.

We present the results of our ablation study in Table 5 and Table 6, for the task of sample generation and interventional generation respectively. Our findings indicate that Cond-FiP decoder trained for both linear and non-linear functional relationships is able to specialize for both the scenarios. While Cond-FiP (LIN) is only able to perform well for linear benchmarks, and similarly Cond-FiP (RFF) can only achieve decent predictions for non-linear benchmarks, Cond-FiP is achieve the best performances on both the linear and non-linear benchmarks.

| Method | Total Nodes | LIN **IN** | RFF **IN** | LIN **OUT** | RFF **OUT** |
|---|---|---|---|---|---|
| `Cond-FiP`(LIN) | 10 | 0.07 (0.02) | 0.4 (0.06) | 0.07 (0.01) | 0.25 (0.06) |
| `Cond-FiP`(RFF) | 10 | 0.1 (0.02) | 0.15 (0.02) | 0.08 (0.01) | 0.09 (0.01) |
| `Cond-FiP` | 10 | 0.06 (0.01) | 0.14 (0.02) | 0.05 (0.01) | 0.08 (0.01) |
| `Cond-FiP`(LIN) | 20 | 0.07 (0.01) | 0.44 (0.07) | 0.10 (0.01) | 0.58 (0.02) |
| `Cond-FiP`(RFF) | 20 | 0.11 (0.01) | 0.26 (0.06) | 0.14 (0.01) | 0.31 (0.03) |
| `Cond-FiP` | 20 | 0.05 (0.01) | 0.24 (0.06) | 0.07 (0.01) | 0.3 (0.03) |
| `Cond-FiP`(LIN) | 50 | 0.10 (0.01) | 0.5 (0.07) | 0.14 (0.02) | 0.69 (0.04) |
| `Cond-FiP`(RFF) | 50 | 0.15 (0.02) | 0.27 (0.05) | 0.19 (0.02) | 0.5 (0.07) |
| `Cond-FiP` | 50 | 0.08 (0.01) | 0.25 (0.05) | 0.07 (0.0) | 0.48 (0.07) |
| `Cond-FiP`(LIN) | 100 | 0.1 (0.01) | 0.51 (0.07) | 0.15 (0.02) | 0.72 (0.04) |
| `Cond-FiP`(RFF) | 100 | 0.16 (0.03) | 0.29 (0.07) | 0.27 (0.04) | 0.59 (0.06) |
| `Cond-FiP` | 100 | 0.07 (0.01) | 0.29 (0.07) | 0.09 (0.01) | 0.57 (0.07) |

Table 5: **Decoder Ablation for Sample Generation.** We compare Cond-FiP for the task of generating samples from input noise variables against two variants. One variant corresponds to a decoder trained on SCMs with only linear functional relationships, `Cond-FiP`(LIN). Similarly, we have another variant where the decoder was trained on SCMs with only rff functional relationships, `Cond-FiP`(RFF). Each cell reports the mean (standard error) RMSE over the multiple test datasets for each scenario.

| Method | Total Nodes | LIN **IN** | RFF **IN** | LIN **OUT** | RFF **OUT** |
|---|---|---|---|---|---|
| `Cond-FiP`(LIN) | 10 | 0.09 (0.02) | 0.40 (0.07) | 0.06 (0.01) | 0.22 (0.04) |
| `Cond-FiP`(RFF) | 10 | 0.16 (0.05) | 0.22 (0.03) | 0.08 (0.01) | 0.11 (0.01) |
| `Cond-FiP` | 10 | 0.10 (0.03) | 0.21 (0.03) | 0.07 (0.01) | 0.11 (0.01) |
| `Cond-FiP`(LIN) | 20 | 0.10 (0.01) | 0.45 (0.07) | 0.16 (0.03) | 0.57 (0.02) |
| `Cond-FiP`(RFF) | 20 | 0.14 (0.02) | 0.26 (0.05) | 0.21 (0.03) | 0.32 (0.02) |
| `Cond-FiP` | 20 | 0.09 (0.01) | 0.24 (0.05) | 0.14 (0.03) | 0.31 (0.03) |
| `Cond-FiP`(LIN) | 50 | 0.14 (0.02) | 0.49 (0.07) | 0.14 (0.02) | 0.68 (0.04) |
| `Cond-FiP`(RFF) | 50 | 0.19 (0.03) | 0.28 (0.05) | 0.21 (0.03) | 0.49 (0.06) |
| `Cond-FiP` | 50 | 0.13 (0.02) | 0.27 (0.04) | 0.12 (0.02) | 0.48 (0.07) |
| `Cond-FiP`(LIN) | 100 | 0.12 (0.02) | 0.52 (0.07) | 0.18 (0.03) | 0.71 (0.04) |
| `Cond-FiP`(RFF) | 100 | 0.18 (0.03) | 0.32 (0.07) | 0.24 (0.04) | 0.59 (0.07) |
| `Cond-FiP` | 100 | 0.10 (0.01) | 0.30 (0.06) | 0.14 (0.02) | 0.58 (0.07) |

Table 6: **Decoder Ablation for Interventional Generation.** We compare Cond-FiP against two variants for the task of interventional data from input noise variables. One variant corresponds to a decoder trained on SCMs with only linear functional relationships, `Cond-FiP`(LIN). Similarly, we have another variant where the decoder was trained on SCMs with only rff functional relationships, `Cond-FiP`(RFF). Each cell reports the mean (standard error) RMSE over the multiple test datasets for each scenario.

## C Evaluating generalization of Cond-FiP to larger sample size

In the main tables (Table 1, Table 5, and Table 3), we evaluated Cond-FiP's generalization capabilities to larger graphs ($d = 50$, $d = 100$) than those used for training ($d = 20$). In this section, we carry a similar experiment where instead of increasing the total nodes in the graph, we test Cond-FiP on datasets with more samples $n_{\text{test}} = 1000$, while Cond-FiP was only trained for datasets with sample size $n_{\text{train}} = 400$.

The results for the experiments are presented in Table 7, Table 8, and Table 9 for the task of noise prediction, sample generation, and interventional generation respectively. Our findings indicate that Cond-FiP is still able to compete with other baseline in this regime. However, we observe that the performances of Cond-FiP did not improve by increasing the sample size compared to the results obtained for the 400 samples case, meaning that the performance of our models depends exclusively on the setting used at training time. We leave for future works the learning of a larger instance of Cond-FiP trained on larger sample size problems.

| Method | Total Nodes | LIN **IN** | RFF **IN** | LIN **OUT** | RFF **OUT** |
|---|---|---|---|---|---|
| `DoWhy` | 10 | 0.02 (0.0) | 0.10 (0.01) | 0.21 (0.04) | 0.23 (0.02) |
| `DECI` | 10 | 0.05 (0.01) | 0.12 (0.01) | 0.21 (0.04) | 0.27 (0.03) |
| `FiP` | 10 | 0.03 (0.0) | 0.06 (0.0) | 0.21 (0.04) | 0.23 (0.02) |
| `Cond-FiP` | 10 | 0.05 (0.01) | 0.11 (0.01) | 0.21 (0.04) | 0.25 (0.02) |
| `DoWhy` | 20 | 0.02 (0.0) | 0.11 (0.02) | 0.16 (0.01) | 0.3 (0.02) |
| `DECI` | 20 | 0.04 (0.01) | 0.11 (0.02) | 0.16 (0.01) | 0.29 (0.02) |
| `FiP` | 20 | 0.03 (0.0) | 0.08 (0.02) | 0.16 (0.01) | 0.26 (0.02) |
| `Cond-FiP` | 20 | 0.06 (0.01) | 0.09 (0.01) | 0.18 (0.01) | 0.26 (0.01) |

Table 7: **Results for Noise Prediction with Larger Sample Size ($n_{\text{test}} = 1000$).** We compare Cond-FiP against the baselines for the task of predicting noise variables from the input observations. Each cell reports the mean (standard error) RMSE over the multiple test datasets for each scenario.

| Method | Total Nodes | LIN **IN** | RFF **IN** | LIN **OUT** | RFF **OUT** |
|---|---|---|---|---|---|
| `DoWhy` | 10 | 0.04 (0.0) | 0.14 (0.02) | 0.29 (0.04) | 0.3 (0.03) |
| `DECI` | 10 | 0.07 (0.01) | 0.17 (0.02) | 0.29 (0.04) | 0.33 (0.04) |
| `FiP` | 10 | 0.05 (0.0) | 0.09 (0.01) | 0.29 (0.04) | 0.29 (0.03) |
| `Cond-FiP` | 10 | 0.05 (0.01) | 0.14 (0.02) | 0.29 (0.04) | 0.29 (0.03) |
| `DoWhy` | 20 | 0.04 (0.01) | 0.21 (0.05) | 0.28 (0.01) | 0.55 (0.06) |
| `DECI` | 20 | 0.07 (0.01) | 0.21 (0.04) | 0.29 (0.01) | 0.59 (0.06) |
| `FiP` | 20 | 0.05 (0.0) | 0.17 (0.04) | 0.28 (0.01) | 0.53 (0.06) |
| `Cond-FiP` | 20 | 0.05 (0.0) | 0.24 (0.05) | 0.28 (0.01) | 0.53 (0.06) |

Table 8: **Results for Sample Generation with Larger Sample Size ($n_{\text{test}} = 1000$).** We compare Cond-FiP against the baselines for the task of generating samples from the input noise variables. Each cell reports the mean (standard error) RMSE over the multiple test datasets for each scenario.

| Method | Total Nodes | LIN **IN** | RFF **IN** | LIN **OUT** | RFF **OUT** |
|---|---|---|---|---|---|
| `DoWhy` | 10 | 0.04 (0.01) | 0.16 (0.03) | 0.26 (0.03) | 0.27 (0.03) |
| `DECI` | 10 | 0.09 (0.01) | 0.19 (0.02) | 0.26 (0.03) | 0.31 (0.04) |
| `FiP` | 10 | 0.05 (0.01) | 0.12 (0.02) | 0.26 (0.03) | 0.27 (0.03) |
| `Cond-FiP` | 10 | 0.09 (0.02) | 0.19 (0.03) | 0.27 (0.03) | 0.3 (0.03) |
| `DoWhy` | 20 | 0.04 (0.0) | 0.20 (0.04) | 0.26 (0.01) | 0.53 (0.06) |
| `DECI` | 20 | 0.08 (0.01) | 0.20 (0.03) | 0.29 (0.02) | 0.54 (0.05) |
| `FiP` | 20 | 0.06 (0.01) | 0.16 (0.04) | 0.28 (0.02) | 0.48 (0.06) |
| `Cond-FiP` | 20 | 0.07 (0.01) | 0.27 (0.05) | 0.30 (0.02) | 0.51 (0.06) |

Table 9: **Results for Interventional Generation with Larger Sample Size ($n_{\text{test}} = 1000$).** We compare Cond-FiP against the baselines for the task of generating interventional data from the input noise variables. Each cell reports the mean (standard error) RMSE over the multiple test datasets for each scenario.

## D Rebuttal Experiments

### D.1 Results without true graph

Our results in the main paper (Table 1, Table 2, Table 3) require the knowledge of true graph ($\mathcal{G}$) as part of the input context to Cond-FiP. In this section we conduct where we don't provide the true graph in the input context, rather we infer the graph $\hat{\mathcal{G}}$ using an amortized causal discovery approach (AVICI (Lorch et al., 2022)) from the observational data $D_{\boldsymbol{X}}$. We chose AVICI for this task since it can enable to infer the graph in a zero-shot manner, hence allowing the combined pipeline of AVICI + Cond-FiP to be a zero-shot technique for learning SCMs. More precisely, AVICI zero-shot infers the graph $\mathcal{G}$ from input context $D_{\boldsymbol{X}}$, and we pass $(\hat{\mathcal{G}}, D_{\boldsymbol{X}})$ as the input context for Cond-FiP. Therefore, for any $\boldsymbol{z} \in \mathbb{R}^d$, Cond-FiP ( $\mathcal{T}(\boldsymbol{z}, D_{\boldsymbol{X}}, \hat{\mathcal{G}})$) aims to replicate the functional mechanism $\boldsymbol{F}(\boldsymbol{z})$ of the underlying SCM.

The results for benchmarking Cond-FiP with inferred graphs using AVICI for the task of noise prediction, sample generation, and interventional generation are provided in Table 10, Table 11, and Table 12 respectively. For a fair comparison, the baselines FiP, DECI, and DoWhy also use the inferred graph ($\hat{\mathcal{G}}$) by AVICI instead of the true graph ($\mathcal{G}$). We find that Cond-FiP remains competitive to baselines even for the scenario of unknown true causal graph. Hence, our amortized training procedure can be extended easily for zero-shot inference of both graphs and causal mechanisms of the SCM.

| Method | Total Nodes | LIN **IN** | RFF **IN** | LIN **OUT** | RFF **OUT** |
|---|---|---|---|---|---|
| `DoWhy` | 10 | 0.16 (0.05) | 0.24 (0.04) | 0.12 (0.03) | 0.12 (0.02) |
| `DECI` | 10 | 0.21 (0.05) | 0.29 (0.04) | 0.16 (0.03) | 0.19 (0.04) |
| `FiP` | 10 | 0.16 (0.05) | 0.2 (0.04) | 0.13 (0.03) | 0.09 (0.01) |
| `Cond-FiP` | 10 | 0.15 (0.05) | 0.2 (0.04) | 0.13 (0.03) | 0.11 (0.01) |
| `DoWhy` | 20 | 0.19 (0.05) | 0.22 (0.03) | 0.2 (0.03) | 0.26 (0.01) |
| `DECI` | 20 | 0.23 (0.05) | 0.28 (0.03) | 0.24 (0.04) | 0.28 (0.02) |
| `FiP` | 20 | 0.2 (0.05) | 0.2 (0.03) | 0.21 (0.03) | 0.21 (0.02) |
| `Cond-FiP` | 20 | 0.18 (0.05) | 0.17 (0.02) | 0.21 (0.03) | 0.16 (0.02) |
| `DoWhy` | 50 | 0.44 (0.05) | 0.3 (0.03) | 0.51 (0.03) | 0.38 (0.04) |
| `DECI` | 50 | 0.46 (0.05) | 0.33 (0.04) | 0.52 (0.03) | 0.42 (0.05) |
| `FiP` | 50 | 0.44 (0.05) | 0.28 (0.04) | 0.51 (0.03) | 0.35 (0.05) |
| `Cond-FiP` | 50 | 0.43 (0.05) | 0.24 (0.03) | 0.53 (0.03) | 0.29 (0.04) |
| `DoWhy` | 100 | 0.49 (0.06) | 0.38 (0.03) | 0.64 (0.03) | 0.53 (0.04) |
| `DECI` | 100 | 0.5 (0.06) | 0.41 (0.03) | 0.64 (0.03) | 0.55 (0.03) |
| `FiP` | 100 | 0.49 (0.06) | 0.37 (0.03) | 0.64 (0.03) | 0.51 (0.04) |
| `Cond-FiP` | 100 | 0.48 (0.06) | 0.34 (0.03) | 0.64 (0.03) | 0.49 (0.04) |

Table 10: **Results for Noise Prediction without True Graph.** We compare Cond-FiP against the baselines for the task of predicting noise variable from input observations. Unlike experiments in the main paper, we do not use the true graph, and infer the **graph first in a zero-shot manner** using AVICI (Lorch et al., 2022). Each cell reports the mean (standard error) RMSE over the multiple test datasets for each scenario. Shaded rows deonte the case where the graph size is larger than the train graph sizes ($d = 20$) for Cond-FiP.

| Method | Total Nodes | LIN **IN** | RFF **IN** | LIN **OUT** | RFF **OUT** |
|---|---|---|---|---|---|
| DoWhy | 10 | 0.22 (0.07) | 0.29 (0.05) | 0.13 (0.04) | 0.14 (0.02) |
| DECI | 10 | 0.29 (0.06) | 0.39 (0.05) | 0.18 (0.04) | 0.22 (0.05) |
| FiP | 10 | 0.23 (0.06) | 0.26 (0.05) | 0.15 (0.04) | 0.12 (0.02) |
| Cond-FiP | 10 | 0.22 (0.07) | 0.26 (0.05) | 0.13 (0.04) | 0.11 (0.02) |
| DoWhy | 20 | 0.25 (0.05) | 0.38 (0.06) | 0.29 (0.06) | 0.42 (0.03) |
| DECI | 20 | 0.3 (0.06) | 0.52 (0.07) | 0.34 (0.06) | 0.47 (0.04) |
| FiP | 20 | 0.26 (0.05) | 0.37 (0.07) | 0.3 (0.06) | 0.33 (0.04) |
| Cond-FiP | 20 | 0.24 (0.05) | 0.36 (0.06) | 0.29 (0.06) | 0.35 (0.03) |
| DoWhy | 50 | 0.53 (0.07) | 0.46 (0.06) | 0.58 (0.03) | 0.59 (0.07) |
| DECI | 50 | 0.55 (0.07) | 0.54 (0.07) | 0.59 (0.02) | 0.66 (0.06) |
| FiP | 50 | 0.53 (0.07) | 0.44 (0.05) | 0.58 (0.02) | 0.53 (0.07) |
| Cond-FiP | 50 | 0.52 (0.07) | 0.43 (0.05) | 0.58 (0.02) | 0.53 (0.07) |
| DoWhy | 100 | 0.67 (0.07) | 0.52 (0.06) | 0.69 (0.02) | 0.68 (0.04) |
| DECI | 100 | 0.69 (0.08) | 0.57 (0.08) | 0.69 (0.02) | 0.71 (0.04) |
| FiP | 100 | 0.66 (0.07) | 0.5 (0.07) | 0.68 (0.02) | 0.64 (0.05) |
| Cond-FiP | 100 | 0.64 (0.06) | 0.49 (0.06) | 0.68 (0.02) | 0.63 (0.05) |

Table 11: **Results for Sample Generation without True Graph.** We compare Cond-FiP against the baselines for the task of generating samples from the input noise variable. Unlike experiments in the main paper, we do not use the true graph, and infer the **graph first in a zero-shot manner** using AVICI (Lorch et al., 2022). Each cell reports the mean (standard error) RMSE over the multiple test datasets for each scenario. Shaded rows deonte the case where the graph size is larger than the train graph sizes ($d = 20$) for Cond-FiP.

| Method | Total Nodes | LIN **IN** | RFF **IN** | LIN **OUT** | RFF **OUT** |
|---|---|---|---|---|---|
| DoWhy | 10 | 0.32 (0.09) | 0.3 (0.05) | 0.13 (0.04) | 0.13 (0.02) |
| DECI | 10 | 0.37 (0.08) | 0.39 (0.05) | 0.17 (0.03) | 0.21 (0.04) |
| FiP | 10 | 0.32 (0.08) | 0.27 (0.05) | 0.14 (0.04) | 0.1 (0.02) |
| Cond-FiP | 10 | 0.31 (0.08) | 0.3 (0.05) | 0.14 (0.04) | 0.13 (0.02) |
| DoWhy | 20 | 0.29 (0.06) | 0.38 (0.07) | 0.37 (0.05) | 0.4 (0.03) |
| DECI | 20 | 0.34 (0.06) | 0.51 (0.07) | 0.41 (0.05) | 0.43 (0.03) |
| FiP | 20 | 0.3 (0.06) | 0.37 (0.07) | 0.38 (0.05) | 0.31 (0.03) |
| Cond-FiP | 20 | 0.29 (0.06) | 0.37 (0.06) | 0.37 (0.05) | 0.33 (0.03) |
| DoWhy | 50 | 0.54 (0.08) | 0.45 (0.06) | 0.62 (0.04) | 0.57 (0.06) |
| DECI | 50 | 0.57 (0.08) | 0.52 (0.07) | 0.63 (0.03) | 0.64 (0.06) |
| FiP | 50 | 0.55 (0.08) | 0.43 (0.05) | 0.62 (0.03) | 0.51 (0.07) |
| Cond-FiP | 50 | 0.54 (0.08) | 0.43 (0.05) | 0.62 (0.03) | 0.51 (0.06) |
| DoWhy | 100 | 0.66 (0.06) | 0.52 (0.07) | 0.71 (0.05) | 0.65 (0.05) |
| DECI | 100 | 0.68 (0.07) | 0.58 (0.09) | 0.71 (0.05) | 0.7 (0.04) |
| FiP | 100 | 0.65 (0.06) | 0.51 (0.07) | 0.71 (0.05) | 0.62 (0.05) |
| Cond-FiP | 100 | 0.64 (0.06) | 0.49 (0.06) | 0.7 (0.04) | 0.62 (0.05) |

Table 12: **Results for Interventional Generation without True Graph.** We compare Cond-FiP against the baselines for the task of interventional data from the input noise variable. Unlike experiments in the main paper, we do not use the true graph, and infer the **graph first in a zero-shot manner** using AVICI (Lorch et al., 2022). Each cell reports the mean (standard error) RMSE over the multiple test datasets for each scenario. Shaded rows deonte the case where the graph size is larger than the train graph sizes ($d = 20$) for Cond-FiP.

## D.2 Evaluating Generalization of Cond-FiP to Smaller Sample Size

### D.2.1 Experiments with $n_{\text{test}} = 100$

In this section we benchmark Cond-FiP against the baselines for the scenario when test datasets in the input context have smaller sample size ($n_{\text{test}} = 100$) as compared to the train datasets ($n_{\text{test}} = 400$).

We report the results for the task of noise prediction, sample generation, and interventional generation in Table 13, Table 14, and Table 15 respectively. We find that Cond-FiP exhibits superior generalization as compared to baselines. For example, in the case of RFF **IN**, Cond-FiP is even better than FiP for all the tasks! This can be attributed to the advantage of zero-shot inference; as the sample size in test dataset decreases, the generalization of baselines would be affected a lot since they require training from scratch on these datasets. However, zero-shot inference methods would be impacted less as they do not have to trained from scratch, and the inductive bias learned by them can help them generalize even with smaller input context.

| Method | Total Nodes | LIN **IN** | RFF **IN** | LIN **OUT** | RFF **OUT** |
|---|---|---|---|---|---|
| `DoWhy` | 10 | 0.06 (0.01) | 0.22 (0.03) | 0.09 (0.01) | 0.16 (0.03) |
| `DECI` | 10 | 0.15 (0.01) | 0.3 (0.02) | 0.22 (0.01) | 0.3 (0.03) |
| `FiP` | 10 | 0.07 (0.01) | 0.18 (0.01) | 0.12 (0.01) | 0.11 (0.01) |
| `Cond-FiP` | 10 | 0.07 (0.01) | 0.14 (0.01) | 0.09 (0.01) | 0.14 (0.01) |
| `DoWhy` | 20 | 0.06 (0.01) | 0.27 (0.05) | 0.07 (0.01) | 0.37 (0.01) |
| `DECI` | 20 | 0.15 (0.02) | 0.33 (0.02) | 0.17 (0.02) | 0.35 (0.03) |
| `FiP` | 20 | 0.09 (0.01) | 0.21 (0.03) | 0.1 (0.01) | 0.27 (0.03) |
| `Cond-FiP` | 20 | 0.08 (0.01) | 0.12 (0.01) | 0.1 (0.01) | 0.15 (0.01) |
| `DoWhy` | 50 | 0.06 (0.01) | 0.29 (0.04) | 0.05 (0.01) | 0.47 (0.04) |
| `DECI` | 50 | 0.14 (0.01) | 0.33 (0.02) | 0.14 (0.02) | 0.4 (0.03) |
| `FiP` | 50 | 0.08 (0.01) | 0.23 (0.03) | 0.08 (0.01) | 0.37 (0.04) |
| `Cond-FiP` | 50 | 0.08 (0.0) | 0.12 (0.01) | 0.08 (0.01) | 0.15 (0.01) |
| `DoWhy` | 100 | 0.06 (0.01) | 0.31 (0.04) | 0.06 (0.01) | 0.5 (0.03) |
| `DECI` | 100 | 0.13 (0.01) | 0.36 (0.03) | 0.12 (0.02) | 0.44 (0.02) |
| `FiP` | 100 | 0.08 (0.01) | 0.25 (0.04) | 0.1 (0.01) | 0.39 (0.03) |
| `Cond-FiP` | 100 | 0.07 (0.0) | 0.13 (0.01) | 0.08 (0.01) | 0.17 (0.01) |

Table 13: **Results for Noise Prediction with Smaller Sample Size ($n_{\text{test}} = 100$).** We compare Cond-FiP against the baselines for the task of predicting noise variable from input observations. Each test dataset contains 100 samples, as opposed to 400 samples in the main paper. Each cell reports the mean (standard error) RMSE over the multiple test datasets for each scenario. Shaded rows deonte the case where the graph size is larger than the train graph sizes ($d = 20$) for Cond-FiP.

### D.2.2 Experiments with $n_{\text{test}} = 50$

We conduct more experiments for the smaller sample size scenarios, where decrease the sample size even further to $n_{\text{test}} = 50$ samples. We report the results for the task of noise prediction, sample generation, and interventional generation in Table 16, Table 17, and Table 18 respectively. We find that baselines perform much worse than Cond-FiP for the all different SCM distributions, highlighting the efficacy of Cond-FiP for inferring functional relationships when the input context has smaller sample size. Note that there were issues with training DoWhy for such a small dataset, hence we do not consider them for this scenario.

| Method | Total Nodes | LIN **IN** | RFF **IN** | LIN **OUT** | RFF **OUT** |
|---|---|---|---|---|---|
| DoWhy | 10 | 0.1 (0.01) | 0.3 (0.06) | 0.12 (0.02) | 0.19 (0.03) |
| DECI | 10 | 0.23 (0.01) | 0.45 (0.04) | 0.31 (0.02) | 0.38 (0.04) |
| FiP | 10 | 0.13 (0.01) | 0.29 (0.04) | 0.18 (0.02) | 0.15 (0.03) |
| Cond-FiP | 10 | 0.09 (0.01) | 0.2 (0.03) | 0.09 (0.02) | 0.14 (0.02) |
| DoWhy | 20 | 0.11 (0.01) | 0.47 (0.15) | 0.11 (0.02) | 0.5 (0.03) |
| DECI | 20 | 0.26 (0.02) | 0.53 (0.05) | 0.26 (0.03) | 0.57 (0.04) |
| FiP | 20 | 0.17 (0.02) | 0.34 (0.06) | 0.17 (0.02) | 0.39 (0.03) |
| Cond-FiP | 20 | 0.08 (0.0) | 0.31 (0.06) | 0.13 (0.01) | 0.37 (0.02) |
| DoWhy | 50 | 0.11 (0.01) | 0.42 (0.08) | 0.09 (0.01) | 0.66 (0.06) |
| DECI | 50 | 0.23 (0.02) | 0.59 (0.08) | 0.27 (0.04) | 0.73 (0.06) |
| FiP | 50 | 0.13 (0.01) | 0.38 (0.07) | 0.14 (0.01) | 0.58 (0.06) |
| Cond-FiP | 50 | 0.1 (0.01) | 0.32 (0.05) | 0.12 (0.01) | 0.54 (0.05) |
| DoWhy | 100 | 0.11 (0.01) | 0.44 (0.08) | 0.11 (0.01) | 0.74 (0.05) |
| DECI | 100 | 0.25 (0.02) | 0.62 (0.08) | 0.25 (0.01) | 0.78 (0.07) |
| FiP | 100 | 0.15 (0.01) | 0.4 (0.07) | 0.19 (0.02) | 0.67 (0.07) |
| Cond-FiP | 100 | 0.11 (0.01) | 0.35 (0.07) | 0.14 (0.02) | 0.63 (0.07) |

Table 14: **Results for Sample Generation with Smaller Sample Size** ($n_{\text{test}} = 100$)**.** We compare Cond-FiP against the baselines for the task of generating samples from the input noise variable. Each test dataset contains $100$ samples, as opposed to $400$ samples in the main paper. Each cell reports the mean (standard error) RMSE over the multiple test datasets for each scenario. Shaded rows deonte the case where the graph size is larger than the train graph sizes ($d = 20$) for Cond-FiP.

| Method | Total Nodes | LIN **IN** | RFF **IN** | LIN **OUT** | RFF **OUT** |
|---|---|---|---|---|---|
| DoWhy | 10 | 0.09 (0.01) | 0.34 (0.08) | 0.11 (0.01) | 0.2 (0.04) |
| DECI | 10 | 0.24 (0.02) | 0.43 (0.04) | 0.26 (0.03) | 0.35 (0.04) |
| FiP | 10 | 0.13 (0.01) | 0.29 (0.04) | 0.14 (0.02) | 0.14 (0.03) |
| Cond-FiP | 10 | 0.09 (0.02) | 0.21 (0.03) | 0.09 (0.01) | 0.12 (0.02) |
| DoWhy | 20 | 0.1 (0.01) | 0.37 (0.08) | 0.11 (0.02) | 0.49 (0.04) |
| DECI | 20 | 0.25 (0.03) | 0.5 (0.05) | 0.28 (0.03) | 0.54 (0.04) |
| FiP | 20 | 0.16 (0.01) | 0.33 (0.06) | 0.2 (0.03) | 0.38 (0.03) |
| Cond-FiP | 20 | 0.1 (0.01) | 0.27 (0.05) | 0.15 (0.02) | 0.29 (0.03) |
| DoWhy | 50 | 0.12 (0.02) | 0.49 (0.14) | 0.09 (0.01) | 0.64 (0.07) |
| DECI | 50 | 0.26 (0.03) | 0.56 (0.07) | 0.26 (0.03) | 0.72 (0.06) |
| FiP | 50 | 0.16 (0.02) | 0.36 (0.06) | 0.15 (0.01) | 0.57 (0.06) |
| Cond-FiP | 50 | 0.13 (0.02) | 0.29 (0.04) | 0.12 (0.01) | 0.49 (0.07) |
| DoWhy | 100 | 0.11 (0.01) | 0.46 (0.07) | 0.11 (0.01) | 1.16 (0.38) |
| DECI | 100 | 0.24 (0.02) | 0.62 (0.08) | 0.26 (0.01) | 0.78 (0.07) |
| FiP | 100 | 0.16 (0.02) | 0.39 (0.07) | 0.2 (0.02) | 0.66 (0.07) |
| Cond-FiP | 100 | 0.12 (0.02) | 0.32 (0.07) | 0.13 (0.01) | 0.58 (0.07) |

Table 15: **Results for Interventional Generation with Smaller Sample Size** ($n_{\text{test}} = 100$)**.** We compare Cond-FiP against the baselines for the task of generating interventional data from the input noise variable. Each test dataset contains $100$ samples, as opposed to $400$ samples in the main paper. Each cell reports the mean (standard error) RMSE over the multiple test datasets for each scenario. Shaded rows deonte the case where the graph size is larger than the train graph sizes ($d = 20$) for Cond-FiP.

| Method | Total Nodes | LIN **IN** | RFF **IN** | LIN **OUT** | RFF **OUT** |
|---|---|---|---|---|---|
| DECI | 10 | 0.19 (0.02) | 0.41 (0.03) | 0.2 (0.02) | 0.42 (0.04) |
| FiP | 10 | 0.13 (0.03) | 0.27 (0.03) | 0.15 (0.02) | 0.21 (0.03) |
| Cond-FiP | 10 | 0.09 (0.01) | 0.17 (0.01) | 0.11 (0.01) | 0.16 (0.01) |
| DECI | 20 | 0.2 (0.01) | 0.42 (0.03) | 0.25 (0.04) | 0.45 (0.05) |
| FiP | 20 | 0.12 (0.01) | 0.33 (0.04) | 0.15 (0.02) | 0.35 (0.04) |
| Cond-FiP | 20 | 0.1 (0.01) | 0.16 (0.01) | 0.11 (0.01) | 0.17 (0.01) |
| DECI | 50 | 0.2 (0.02) | 0.43 (0.02) | 0.2 (0.03) | 0.5 (0.05) |
| FiP | 50 | 0.13 (0.01) | 0.32 (0.03) | 0.13 (0.01) | 0.49 (0.05) |
| Cond-FiP | 50 | 0.1 (0.01) | 0.16 (0.0) | 0.1 (0.01) | 0.17 (0.01) |
| DECI | 100 | 0.19 (0.02) | 0.43 (0.03) | 0.21 (0.01) | 0.53 (0.02) |
| FiP | 100 | 0.11 (0.01) | 0.32 (0.04) | 0.13 (0.01) | 0.48 (0.02) |
| Cond-FiP | 100 | 0.09 (0.01) | 0.16 (0.01) | 0.09 (0.01) | 0.18 (0.01) |

Table 16: **Results for Noise Prediction with Smaller Sample Size ($n_{\text{test}} = 50$).** We compare Cond-FiP against the baselines for the task of predicting noise variable from input observations. Each test dataset contains $50$ samples, as opposed to $400$ samples in the main paper. Each cell reports the mean (standard error) RMSE over the multiple test datasets for each scenario. Shaded rows deonte the case where the graph size is larger than the train graph sizes ($d = 20$) for Cond-FiP.

| Method | Total Nodes | LIN **IN** | RFF **IN** | LIN **OUT** | RFF **OUT** |
|---|---|---|---|---|---|
| DECI | 10 | 0.31 (0.02) | 0.58 (0.05) | 0.27 (0.04) | 0.49 (0.07) |
| FiP | 10 | 0.2 (0.03) | 0.4 (0.05) | 0.21 (0.03) | 0.25 (0.04) |
| Cond-FiP | 10 | 0.12 (0.02) | 0.28 (0.03) | 0.12 (0.01) | 0.18 (0.03) |
| DECI | 20 | 0.34 (0.02) | 0.66 (0.08) | 0.39 (0.07) | 0.68 (0.05) |
| FiP | 20 | 0.2 (0.01) | 0.51 (0.08) | 0.25 (0.04) | 0.51 (0.02) |
| Cond-FiP | 20 | 0.13 (0.01) | 0.4 (0.06) | 0.19 (0.02) | 0.43 (0.02) |
| DECI | 50 | 0.32 (0.02) | 0.66 (0.06) | 0.36 (0.02) | 0.8 (0.06) |
| FiP | 50 | 0.2 (0.01) | 0.48 (0.07) | 0.22 (0.02) | 0.69 (0.06) |
| Cond-FiP | 50 | 0.15 (0.02) | 0.4 (0.05) | 0.16 (0.01) | 0.59 (0.06) |
| DECI | 100 | 0.36 (0.04) | 0.68 (0.08) | 0.39 (0.03) | 0.84 (0.06) |
| FiP | 100 | 0.2 (0.02) | 0.49 (0.09) | 0.28 (0.03) | 0.73 (0.07) |
| Cond-FiP | 100 | 0.16 (0.01) | 0.42 (0.07) | 0.22 (0.01) | 0.68 (0.06) |

Table 17: **Results for Sample Generation with Smaller Sample Size ($n_{\text{test}} = 50$).** We compare Cond-FiP against the baselines for the task of generating samples from the input noise variable. Each test dataset contains $50$ samples, as opposed to $400$ samples in the main paper. Each cell reports the mean (standard error) RMSE over the multiple test datasets for each scenario. Shaded rows deonte the case where the graph size is larger than the train graph sizes ($d = 20$) for Cond-FiP.

| Method | Total Nodes | LIN **IN** | RFF **IN** | LIN **OUT** | RFF **OUT** |
|---|---|---|---|---|---|
| DECI | 10 | 0.3 (0.03) | 0.53 (0.05) | 0.26 (0.04) | 0.42 (0.05) |
| FiP | 10 | 0.21 (0.04) | 0.35 (0.04) | 0.2 (0.03) | 0.22 (0.03) |
| Cond-FiP | 10 | 0.12 (0.01) | 0.19 (0.03) | 0.07 (0.01) | 0.14 (0.02) |
| DECI | 20 | 0.33 (0.02) | 0.6 (0.06) | 0.43 (0.07) | 0.63 (0.04) |
| FiP | 20 | 0.21 (0.02) | 0.46 (0.07) | 0.29 (0.04) | 0.49 (0.02) |
| Cond-FiP | 20 | 0.11 (0.01) | 0.29 (0.06) | 0.15 (0.02) | 0.32 (0.03) |
| DECI | 50 | 0.34 (0.02) | 0.66 (0.07) | 0.34 (0.02) | 0.78 (0.06) |
| FiP | 50 | 0.21 (0.02) | 0.46 (0.07) | 0.23 (0.02) | 0.68 (0.06) |
| Cond-FiP | 50 | 0.13 (0.02) | 0.31 (0.05) | 0.12 (0.02) | 0.51 (0.07) |
| DECI | 100 | 0.37 (0.04) | 0.67 (0.08) | 0.4 (0.04) | 0.84 (0.06) |
| FiP | 100 | 0.21 (0.02) | 0.49 (0.08) | 0.28 (0.03) | 0.73 (0.07) |
| Cond-FiP | 100 | 0.12 (0.01) | 0.33 (0.07) | 0.14 (0.01) | 0.58 (0.07) |

Table 18: **Results for Interventional Generation with Smaller Sample Size** ($n_{\text{test}} = 50$)**.** We compare Cond-FiP against the baselines for the task of generating interventional data from the input noise variable. Each test dataset contains $50$ samples, as opposed to $400$ samples in the main paper. Each cell reports the mean (standard error) RMSE over the multiple test datasets for each scenario. Shaded rows deonte the case where the graph size is larger than the train graph sizes ($d = 20$) for Cond-FiP.

### D.3 Ablation Study of Encoder

Similar to the ablation study of decoder Appendix B, we conduct an ablation study where we train two variants of the encoder in Cond-FiP described as follows:

- *Cond-FiP (LIN)*: We sample SCMs with linear functional relationships during training of the encoder.
- *Cond-FiP (RFF)*: We sample SCMs with rff functional relationships during training of the encoder.

Note that for the training the subsequent decoder, we sample SCMs with both linear and rff functional relationships as in the main results ( Table 1, Table 2, and Table 3). Note that in the main results, the encoder was trained by sampling SCMs with both linear and rff functional relationships. Hence, this ablation helps us to understand whether the strategy of training encoder on mixed functional relationships can bring more generalization to the amortization process, or if we should have trained encoders specialized for linear and non-linear functional relationships.

We present our results of the ablation study for the task of noise prediction, sample generation, and interventional generation in Table 19, Table 20, Table 21 respectively. Our findings indicate that Cond-FiP is robust to the choice of encoder training strategy! Even though the encoder for Cond-FiP (LIN) was only trained on data from linear SCMs, its generalization performance is similar to Cond-FiP where the encoder was trained on data from both linear and non-linear SCMs.

| Method | Total Nodes | LIN **IN** | RFF **IN** | LIN **OUT** | RFF **OUT** |
|---|---|---|---|---|---|
| `Cond-FiP`(LIN) | 10 | 0.07 (0.01) | 0.21 (0.02) | 0.08 (0.01) | 0.2 (0.03) |
| `Cond-FiP`(RFF) | 10 | 0.06 (0.01) | 0.11 (0.01) | 0.07 (0.01) | 0.09 (0.01) |
| `Cond-FiP` | 10 | 0.06 (0.01) | 0.1 (0.01) | 0.07 (0.01) | 0.1 (0.01) |
| `Cond-FiP`(LIN) | 20 | 0.07 (0.01) | 0.19 (0.02) | 0.09 (0.01) | 0.21 (0.01) |
| `Cond-FiP`(RFF) | 20 | 0.06 (0.01) | 0.09 (0.01) | 0.1 (0.02) | 0.11 (0.01) |
| `Cond-FiP` | 20 | 0.06 (0.01) | 0.09 (0.01) | 0.07 (0.0) | 0.12 (0.0) |
| `Cond-FiP`(LIN) | 50 | 0.07 (0.01) | 0.21 (0.02) | 0.07 (0.01) | 0.24 (0.01) |
| `Cond-FiP`(RFF) | 50 | 0.07 (0.01) | 0.09 (0.01) | 0.07 (0.0) | 0.14 (0.01) |
| `Cond-FiP` | 50 | 0.06 (0.01) | 0.1 (0.01) | 0.07 (0.01) | 0.14 (0.01) |
| `Cond-FiP`(LIN) | 100 | 0.06 (0.0) | 0.22 (0.02) | 0.07 (0.01) | 0.26 (0.01) |
| `Cond-FiP`(RFF) | 100 | 0.06 (0.01) | 0.09 (0.01) | 0.07 (0.01) | 0.14 (0.01) |
| `Cond-FiP` | 100 | 0.05 (0.0) | 0.1 (0.01) | 0.07 (0.01) | 0.16 (0.01) |

Table 19: **Encoder Ablation for Noise Prediction.** We compare Cond-FiP against the baselines for the task of predicting noise variable from input observations against two variants. One variant corresponds to the encoder trained on SCMs with only linear functional relationships, `Cond-FiP`(LIN). Similarly, we have another variant where the decoder was trained on SCMs with only rff functional relationships, `Cond-FiP`(RFF). Each cell reports the mean (standard error) RMSE over the multiple test datasets for each scenario.

| Method | Total Nodes | LIN **IN** | RFF **IN** | LIN **OUT** | RFF **OUT** |
|---|---|---|---|---|---|
| `Cond-FiP`(LIN) | 10 | 0.05 (0.01) | 0.14 (0.02) | 0.06 (0.0) | 0.08 (0.01) |
| `Cond-FiP`(RFF) | 10 | 0.08 (0.01) | 0.18 (0.06) | 0.06 (0.0) | 0.07 (0.01) |
| `Cond-FiP` | 10 | 0.06 (0.01) | 0.14 (0.02) | 0.05 (0.01) | 0.08 (0.01) |
| `Cond-FiP`(LIN) | 20 | 0.05 (0.01) | 0.25 (0.06) | 0.07 (0.01) | 0.3 (0.03) |
| `Cond-FiP`(RFF) | 20 | 0.08 (0.01) | 0.22 (0.05) | 0.11 (0.01) | 0.29 (0.03) |
| `Cond-FiP` | 20 | 0.05 (0.01) | 0.24 (0.06) | 0.07 (0.01) | 0.3 (0.03) |
| `Cond-FiP`(LIN) | 50 | 0.08 (0.01) | 0.26 (0.05) | 0.11 (0.04) | 0.52 (0.08) |
| `Cond-FiP`(RFF) | 50 | 0.11 (0.01) | 0.26 (0.05) | 0.15 (0.02) | 0.48 (0.07) |
| `Cond-FiP` | 50 | 0.08 (0.01) | 0.25 (0.05) | 0.07 (0.0) | 0.48 (0.07) |
| `Cond-FiP`(LIN) | 100 | 0.07 (0.01) | 0.27 (0.06) | 0.08 (0.0) | 0.57 (0.07) |
| `Cond-FiP`(RFF) | 100 | 0.11 (0.01) | 0.29 (0.08) | 0.18 (0.03) | 0.61 (0.08) |
| `Cond-FiP` | 100 | 0.07 (0.01) | 0.29 (0.07) | 0.09 (0.01) | 0.57 (0.07) |

Table 20: **Encoder Ablation for Sample Generation.** We compare Cond-FiP against the baselines for the task of generating samples from input noise variables against two variants. One variant corresponds to the encoder trained on SCMs with only linear functional relationships, `Cond-FiP`(LIN). Similarly, we have another variant where the decoder was trained on SCMs with only rff functional relationships, `Cond-FiP`(RFF). Each cell reports the mean (standard error) RMSE over the multiple test datasets for each scenario.

| Method | Total Nodes | LIN **IN** | RFF **IN** | LIN **OUT** | RFF **OUT** |
|---|---|---|---|---|---|
| `Cond-FiP`(LIN) | 10 | 0.09 (0.02) | 0.2 (0.03) | 0.06 (0.01) | 0.1 (0.01) |
| `Cond-FiP`(RFF) | 10 | 0.13 (0.04) | 0.23 (0.08) | 0.08 (0.01) | 0.1 (0.01) |
| `Cond-FiP` | 10 | 0.1 (0.03) | 0.21 (0.03) | 0.07 (0.01) | 0.11 (0.01) |
| `Cond-FiP`(LIN) | 20 | 0.08 (0.01) | 0.24 (0.05) | 0.12 (0.04) | 0.3 (0.03) |
| `Cond-FiP`(RFF) | 20 | 0.13 (0.02) | 0.23 (0.05) | 0.13 (0.03) | 0.31 (0.02) |
| `Cond-FiP` | 20 | 0.09 (0.01) | 0.24 (0.05) | 0.14 (0.03) | 0.31 (0.03) |
| `Cond-FiP`(LIN) | 50 | 0.12 (0.02) | 0.29 (0.05) | 0.1 (0.01) | 0.51 (0.07) |
| `Cond-FiP`(RFF) | 50 | 0.14 (0.02) | 0.29 (0.05) | 0.18 (0.03) | 0.47 (0.06) |
| `Cond-FiP` | 50 | 0.13 (0.02) | 0.27 (0.04) | 0.12 (0.02) | 0.48 (0.07) |
| `Cond-FiP`(LIN) | 100 | 0.1 (0.01) | 0.3 (0.06) | 0.12 (0.01) | 0.56 (0.07) |
| `Cond-FiP`(RFF) | 100 | 0.12 (0.01) | 0.31 (0.07) | 0.2 (0.04) | 0.6 (0.09) |
| `Cond-FiP` | 100 | 0.1 (0.01) | 0.3 (0.06) | 0.14 (0.02) | 0.58 (0.07) |

Table 21: **Encoder Ablation for Interventional Generation.** We compare Cond-FiP against the baselines for the task of generating interventional data from input noise variables against two variants. One variant corresponds to the encoder trained on SCMs with only linear functional relationships, `Cond-FiP`(LIN). Similarly, we have another variant where the decoder was trained on SCMs with only rff functional relationships, `Cond-FiP`(RFF). Each cell reports the mean (standard error) RMSE over the multiple test datasets for each scenario.

## D.4 Counterfactual Generation with Cond-FiP

We provide results (Table 22) for bechmarking Cond-FiP against baselines for the task of counterfactual generation. We operate in the same setup as the one in our main results ($n_{\text{test}} = 400$) and all the methods are provided with the true casual graph. We observe that Unlike the tasks of noise prediction, sample & interventional generation, we find that Cond-FiP is worse than the baselines for the task of counterfactual generation. This can be explained as the training of Cond-FiP decoder relies on the true noise variables, and the model struggles to generalize the learned functional mechanisms when provided with inferred noise variables. We leave the improvement of Cond-FiP for counterfactual generation as future work.

| Method | Total Nodes | LIN **IN** | RFF **IN** | LIN **OUT** | RFF **OUT** |
|---|---|---|---|---|---|
| DoWhy | 10 | 0.03 (0.03) | 0.13 (0.03) | 0.0 (0.0) | 0.04 (0.01) |
| DECI | 10 | 0.1 (0.02) | 0.2 (0.03) | 0.04 (0.01) | 0.11 (0.02) |
| FiP | 10 | 0.03 (0.01) | 0.09 (0.02) | 0.02 (0.0) | 0.03 (0.01) |
| Cond-FiP | 10 | 0.09 (0.03) | 0.21 (0.03) | 0.05 (0.01) | 0.11 (0.01) |
| DoWhy | 20 | 0.01 (0.0) | 0.12 (0.03) | 0.0 (0.0) | 0.13 (0.02) |
| DECI | 20 | 0.06 (0.01) | 0.15 (0.03) | 0.07 (0.03) | 0.15 (0.02) |
| FiP | 20 | 0.03 (0.01) | 0.1 (0.03) | 0.06 (0.04) | 0.09 (0.02) |
| Cond-FiP | 20 | 0.09 (0.02) | 0.26 (0.05) | 0.13 (0.02) | 0.3 (0.03) |
| DoWhy | 50 | 0.0 (0.0) | 0.09 (0.02) | 0.0 (0.0) | 0.17 (0.04) |
| DECI | 50 | 0.04 (0.01) | 0.11 (0.02) | 0.03 (0.01) | 0.18 (0.04) |
| FiP | 50 | 0.03 (0.01) | 0.08 (0.02) | 0.03 (0.01) | 0.14 (0.04) |
| Cond-FiP | 50 | 0.1 (0.02) | 0.26 (0.04) | 0.1 (0.01) | 0.46 (0.06) |
| DoWhy | 100 | 0.0 (0.0) | 0.08 (0.02) | 0.0 (0.0) | 0.2 (0.05) |
| DECI | 100 | 0.02 (0.01) | 0.1 (0.02) | 0.02 (0.01) | 0.22 (0.05) |
| FiP | 100 | 0.01 (0.01) | 0.07 (0.02) | 0.02 (0.01) | 0.19 (0.05) |
| Cond-FiP | 100 | 0.09 (0.02) | 0.29 (0.06) | 0.13 (0.02) | 0.56 (0.08) |

Table 22: **Results for Counterfactual Generation.** We compare Cond-FiP against the baselines for the task of generating counterfactual data from the input noise variables. Each cell reports the mean (standard error) RMSE over the multiple test datasets for each scenario. Shaded rows denote the case where the graph size is larger than the train graph sizes ($d = 20$) for Cond-FiP. We observe that Cond-FiP is worse than the baselines, and leave the improvement of Cond-FiP for counterfactual generation as future work.

## D.5 Sensitivity to Distribution Shifts

In our main results (Table 1, 2, 3) we experimented with datasets sampled from SCM following a different distribution (LIN **OUT**, RFF **OUT**) than the datasets used for training Cond-FiP (LIN **IN**, RFF **IN**). As expected, the performance of all methods drop in the presence of distribution shift. We now analyze how sensitive is Cond-FiP to distribution shifts by comparing its performance across scenarios as the severity of the distribution shift is increased.

To illustrate how we control the magnitude of distribution shift, we discuss the difference in the distribution of causal mechanisms across $\mathbb{P}_{\text{IN}}$ and $\mathbb{P}_{\text{OUT}}$. The distribution shift arises because the support of the parameters of causal mechanisms changes from $\mathbb{P}_{\text{IN}}$ to $\mathbb{P}_{\text{OUT}}$. For example, for linear causal mechanism case, the weights in $\mathbb{P}_{\text{IN}}$ are sampled uniformly from $(-3, -1) \cup (1, 3)$; while in $\mathbb{P}_{\text{OUT}}$ they are sampled from uniformly from $(0.5, 4)$. We now change the support set of the parameters in $\mathbb{P}_{\text{OUT}}$ to $0.5\alpha, 4\alpha$, so that by increasing $\alpha$ we make the distribution shift more severe. We follow this procedure for the support set of all the parameters associated with functional mechanisms and generate distributions ($\mathbb{P}_{\text{OUT}}(\alpha)$) with varying shift w.r.t $\mathbb{P}_{\text{IN}}$ by changing $\alpha$. Note that $\alpha = 1$ corresponds to the same $\mathbb{P}_{\text{OUT}}$ as the one used for sampling datasets in our main results.

We conduct two experiments for evaluating the robustness of Cond-FiP to distribution shifts, described ahead.

- **Controlling Shift in Causal Mechanisms.** We start with the parameter configuration of $\mathbb{P}_{\text{OUT}}$ from the setup in main results; and then control the magnitude of shift by changing the support set of parameters of causal mechanisms.
- **Controlling Shift in Noise Variablse.** We start with the parameter configuration of $\mathbb{P}_{\text{OUT}}$ from the setup in main results; and then control the magnitude of shift by changing the support set of parameters of noise distribution.

Tables 23, 24, and 25 provide results for the case of controlling shift via causal mechanisms, for the task of noise prediction, sample generation, and interventional generation respectively. We find that the performance of Cond-FiP does not change much as we increase $\alpha$, indicating that Cond-FiP is robust to the varying levels of distribution shits in causal mechanisms.

However, for the case of controlling shift via noise variables (Table 26, 27, and 28) we find that Cond-FiP is quite sensitive to the varying levels of distribution shift in noise variables. The performance of Cond-FiP degrades with increasing magnitude of the shift ($\alpha$) for all the tasks.

| Total Nodes | Shift Level ($\alpha$) | LIN **OUT** | RFF **OUT** |
|---|---|---|---|
| 10 | 1 | 0.07 (0.01) | 0.10 (0.01) |
| 10 | 2 | 0.06 (0.01) | 0.10 (0.01) |
| 10 | 5 | 0.05 (0.01) | 0.10 (0.01) |
| 10 | 10 | 0.05 (0.01) | 0.10 (0.01) |
| 20 | 1 | 0.07 (0.0) | 0.12 (0.0) |
| 20 | 2 | 0.06 (0.0) | 0.13 (0.01) |
| 20 | 5 | 0.05 (0.0) | 0.11 (0.01) |
| 20 | 10 | 0.05 (0.0) | 0.10 (0.01) |
| 50 | 1 | 0.07 (0.01) | 0.14 (0.01) |
| 50 | 2 | 0.05 (0.01) | 0.17 (0.01) |
| 50 | 5 | 0.05 (0.01) | 0.14 (0.01) |
| 50 | 10 | 0.04 (0.0) | 0.14 (0.01) |
| 100 | 1 | 0.07 (0.01) | 0.16 (0.01) |
| 100 | 2 | 0.05 (0.01) | 0.18 (0.0) |
| 100 | 5 | 0.05 (0.0) | 0.17 (0.01) |
| 100 | 10 | 0.05 (0.0) | 0.16 (0.01) |

Table 23: **Results for Noise Prediction under Distribution Shifts in Causal Mechanisms.** We evaluate the robustness of Cond-FiP to distribution shifts in the parametrization of causal mechanisms. We vary the distribution shift controlled by $\alpha$, where $\alpha = 1$ corresponds to the case in main results Table 1. Each cell reports the mean (standard error) RMSE over the multiple test datasets for each scenario. We find that Cond-FiP is robust to varying levels of distribution shift in causal mechanisms.

| Total Nodes | Shift Level ($\alpha$) | LIN **OUT** | RFF **OUT** |
|---|---|---|---|
| 10 | 1 | 0.05 (0.01) | 0.08 (0.01) |
| 10 | 2 | 0.05 (0.0) | 0.07 (0.01) |
| 10 | 5 | 0.05 (0.0) | 0.07 (0.01) |
| 10 | 10 | 0.06 (0.0) | 0.06 (0.01) |
| 20 | 1 | 0.07 (0.01) | 0.30 (0.03) |
| 20 | 2 | 0.06 (0.01) | 0.34 (0.05) |
| 20 | 5 | 0.06 (0.01) | 0.35 (0.05) |
| 20 | 10 | 0.06 (0.01) | 0.29 (0.07) |
| 50 | 1 | 0.07 (0.0) | 0.48 (0.07) |
| 50 | 2 | 0.07 (0.0) | 0.47 (0.07) |
| 50 | 5 | 0.07 (0.01) | 0.38 (0.06) |
| 50 | 10 | 0.07 (0.01) | 0.32 (0.06) |
| 100 | 1 | 0.09 (0.01) | 0.57 (0.07) |
| 100 | 2 | 0.09 (0.01) | 0.60 (0.05) |
| 100 | 5 | 0.09 (0.01) | 0.58 (0.05) |
| 100 | 10 | 0.12 (0.02) | 0.56 (0.06) |

Table 24: **Results for Sample Generation under Distribution Shifts in Causal Mechanisms.** We evaluate the robustness of Cond-FiP to distribution shifts in the parametrization of causal mechanisms. We vary the distribution shift controlled by $\alpha$, where $\alpha = 1$ corresponds to the case in main results Table 2. Each cell reports the mean (standard error) RMSE over the multiple test datasets for each scenario. We find that Cond-FiP is robust to varying levels of distribution shift in causal mechanisms.

| Total Nodes | Shift Level ($\alpha$) | LIN **OUT** | RFF **OUT** |
|---|---|---|---|
| 10 | 1 | 0.07 (0.01) | 0.11 (0.01) |
| 10 | 2 | 0.07 (0.01) | 0.11 (0.01) |
| 10 | 5 | 0.07 (0.01) | 0.10 (0.01) |
| 10 | 10 | 0.06 (0.01) | 0.10 (0.01) |
| 20 | 1 | 0.14 (0.03) | 0.31 (0.03) |
| 20 | 2 | 0.10 (0.02) | 0.33 (0.04) |
| 20 | 5 | 0.17 (0.1) | 0.34 (0.04) |
| 20 | 10 | 0.10 (0.03) | 0.28 (0.05) |
| 50 | 1 | 0.12 (0.02) | 0.48 (0.07) |
| 50 | 2 | 0.12 (0.03) | 0.47 (0.07) |
| 50 | 5 | 0.11 (0.01) | 0.39 (0.06) |
| 50 | 10 | 0.11 (0.02) | 0.32 (0.06) |
| 100 | 1 | 0.14 (0.02) | 0.58 (0.07) |
| 100 | 2 | 0.13 (0.02) | 0.60 (0.06) |
| 100 | 5 | 0.14 (0.03) | 0.58 (0.05) |
| 100 | 10 | 0.18 (0.04) | 0.55 (0.06) |

Table 25: **Results for Interventional Generation under Distribution Shifts in Causal Mechanisms.** We evaluate the robustness of Cond-FiP to distribution shifts in the parametrization of causal mechanisms. We vary the distribution shift controlled by $\alpha$, where $\alpha = 1$ corresponds to the case in main results Table 3. Each cell reports the mean (standard error) RMSE over the multiple test datasets for each scenario. We find that Cond-FiP is robust to varying levels of distribution shift in causal mechanisms.

| Total Nodes | Shift Level ($\alpha$) | LIN **OUT** | RFF **OUT** |
|---|---|---|---|
| 10 | 1 | 0.07 (0.01) | 0.10 (0.01) |
| 10 | 2 | 0.07 (0.01) | 0.11 (0.01) |
| 10 | 5 | 0.07 (0.01) | 0.18 (0.02) |
| 10 | 10 | 0.08 (0.01) | 0.26 (0.04) |
| 20 | 1 | 0.07 (0.0) | 0.12 (0.0) |
| 20 | 2 | 0.07 (0.0) | 0.16 (0.01) |
| 20 | 5 | 0.07 (0.0) | 0.30 (0.01) |
| 20 | 10 | 0.07 (0.0) | 0.41 (0.02) |
| 50 | 1 | 0.07 (0.01) | 0.14 (0.01) |
| 50 | 2 | 0.07 (0.01) | 0.19 (0.01) |
| 50 | 5 | 0.07 (0.01) | 0.33 (0.02) |
| 50 | 10 | 0.07 (0.01) | 0.44 (0.02) |
| 100 | 1 | 0.07 (0.01) | 0.16 (0.01) |
| 100 | 2 | 0.07 (0.01) | 0.22 (0.0) |
| 100 | 5 | 0.07 (0.01) | 0.35 (0.01) |
| 100 | 10 | 0.07 (0.01) | 0.44 (0.01) |

Table 26: **Results for Noise Prediction under Distribution Shifts in Noise Variables.** We evaluate the robustness of Cond-FiP to distribution shifts in the parametrization of noise distribution. We vary the distribution shift controlled by $\alpha$, where $\alpha = 1$ corresponds to the case in main results Table 1. Each cell reports the mean (standard error) RMSE over the multiple test datasets for each scenario. We find that Cond-FiP is sensitive to varying levels of distribution shift in noise variables, its performance decreases with increasing magnitude of the shift.

| Total Nodes | Shift Level ($\alpha$) | LIN **OUT** | RFF **OUT** |
|---|---|---|---|
| 10 | 1 | 0.05 (0.01) | 0.08 (0.01) |
| 10 | 2 | 0.05 (0.0) | 0.13 (0.03) |
| 10 | 5 | 0.05 (0.01) | 0.28 (0.06) |
| 10 | 10 | 0.05 (0.01) | 0.36 (0.08) |
| 20 | 1 | 0.07 (0.01) | 0.30 (0.03) |
| 20 | 2 | 0.07 (0.01) | 0.45 (0.04) |
| 20 | 5 | 0.07 (0.01) | 0.59 (0.03) |
| 20 | 10 | 0.07 (0.01) | 0.58 (0.02) |
| 50 | 1 | 0.07 (0.0) | 0.48 (0.07) |
| 50 | 2 | 0.07 (0.0) | 0.59 (0.06) |
| 50 | 5 | 0.07 (0.0) | 0.64 (0.03) |
| 50 | 10 | 0.07 (0.0) | 0.58 (0.02) |
| 100 | 1 | 0.09 (0.01) | 0.57 (0.07) |
| 100 | 2 | 0.09 (0.01) | 0.63 (0.05) |
| 100 | 5 | 0.09 (0.01) | 0.65 (0.03) |
| 100 | 10 | 0.09 (0.01) | 0.59 (0.02) |

Table 27: **Results for Sample Generation under Distribution Shifts in Noise Variables.** We evaluate the robustness of Cond-FiP to distribution shifts in the parametrization of noise distribution. We vary the distribution shift controlled by $\alpha$, where $\alpha = 1$ corresponds to the case in main results Table 2. Each cell reports the mean (standard error) RMSE over the multiple test datasets for each scenario. We find that Cond-FiP is sensitive to varying levels of distribution shift in noise variables, its performance decreases with increasing magnitude of the shift.

| Total Nodes | Shift Level ($\alpha$) | LIN **OUT** | RFF **OUT** |
|---|---|---|---|
| 10 | 1 | 0.07 (0.01) | 0.11 (0.01) |
| 10 | 2 | 0.07 (0.01) | 0.14 (0.02) |
| 10 | 5 | 0.07 (0.01) | 0.25 (0.05) |
| 10 | 10 | 0.07 (0.01) | 0.32 (0.06) |
| 20 | 1 | 0.14 (0.03) | 0.31 (0.03) |
| 20 | 2 | 0.14 (0.03) | 0.42 (0.03) |
| 20 | 5 | 0.14 (0.03) | 0.57 (0.03) |
| 20 | 10 | 0.14 (0.03) | 0.56 (0.02) |
| 50 | 1 | 0.12 (0.02) | 0.48 (0.07) |
| 50 | 2 | 0.12 (0.01) | 0.58 (0.06) |
| 50 | 5 | 0.12 (0.01) | 0.65 (0.04) |
| 50 | 10 | 0.12 (0.01) | 0.59 (0.02) |
| 100 | 1 | 0.14 (0.02) | 0.58 (0.07) |
| 100 | 2 | 0.14 (0.02) | 0.65 (0.06) |
| 100 | 5 | 0.14 (0.02) | 0.67 (0.04) |
| 100 | 10 | 0.14 (0.02) | 0.60 (0.03) |

Table 28: **Results for Interventional Generation under Distribution Shifts in Noise Variables.** We evaluate the robustness of Cond-FiP to distribution shifts in the parametrization of noise distribution. We vary the distribution shift controlled by $\alpha$, where $\alpha = 1$ corresponds to the case in main results Table 3. Each cell reports the mean (standard error) RMSE over the multiple test datasets for each scenario. We find that Cond-FiP is sensitive to varying levels of distribution shift in noise variables, its performance decreases with increasing magnitude of the shift.

## E Additional Details on Cond-FiP

### E.1 Amortized Learning in Causal ML

The goal of amortized learning is to learn to predict the solution of similar instances of the same optimization problem. More formally, given some random inputs $\mathbf{I} \sim P_{\mathbf{I}}$ and an objective function $L(\theta, \mathbf{I})$, the goal of amortized learning is to learn a parameterized model $\mathcal{M}_\phi$ s.t.

$$\mathcal{M}_\phi(\mathbf{I}) \simeq \theta^*(\mathbf{I}) := \text{argmin}_{\theta \in \Theta} L(\theta, \mathbf{I})$$

To train such a model, amortized learning requires to have access to various pairs $(\mathbf{I}, \theta^*(\mathbf{I}))$ and optimize the parameters $\phi$ of $\mathcal{M}$ in a supervised manner. In the causal literature, this concept has been employed to learn graphs, topological orders, and even the average treatment effect (ATE) from observations (Zhang et al., 2023; Gupta et al., 2023; Lorch et al., 2022; Ke et al., 2022; Wu et al., 2024; Scetbon et al., 2024). In all these cases, the variable $\mathbf{I}$ denotes a dataset of observations $D_{\mathbf{X}}$ and the target variable $\theta^*(\mathbf{I})$ can represent either the causal graph, the topological order or the ATE depending on the task considered.

In our work, we take this technique a step further by directly predicting functions from datasets (and causal graphs). More formally, in our setting, $\mathbf{I} := (D_{\mathbf{X}}, \mathcal{G})$ and $\theta^*(\mathbf{I}) := \mathbf{F}$ where $\mathbf{F}$ is the true SCM generating $D_{\mathbf{X}}$.

### E.2 Inference with Cond-FiP

**Cond-FiP Model.** Once Cond-FiP is trained, we have access to two trained models: (1) an encoder that given a dataset $D_{\mathbf{X}}$ and the causal graph associated $\mathcal{G}$ produced an embedding $\mu(D_{\mathbf{X}}, \mathcal{G})$ as defined l.277., and (2) a decoder that given an embedding $\mu$ and a causal graph $\mathcal{G}$, produces a function $z \in \mathbb{R}^d \to \mathcal{T}(z, \mu, \mathcal{G}) \in \mathbb{R}^d$.

Cond-FiP simply consists of the composition of the two models, that is given a dataset $D_{\mathbf{X}}$ and the causal graph associated $\mathcal{G}$, produce a function $z \in \mathbb{R}^d \to \mathcal{T}(z, \mu(D_{\mathbf{X}}, \mathcal{G}), \mathcal{G}) \in \mathbb{R}^d$, which for simplicity we denote $z \in \mathbb{R}^d \to \mathcal{T}(z, D_{\mathbf{X}}, \mathcal{G}) \in \mathbb{R}^d$. Having clarified this, we can now proceed to more detailed explanations of the inference process using Cond-FiP.

**Data Generation.** Given a dataset $D_{\boldsymbol{X}}$ and its causal graph $\mathcal{G}$, we denote $z \to \mathcal{T}(z, D_{\boldsymbol{X}}, \mathcal{G})$ the function infered by Cond-FiP. This function defines the predicted SCM obtained by our model, and we can directly use it to generate new points. More precisely, given a noise sample $\mathbf{n}$, we can generate the associated observational sample by solving the following equation in $\mathbf{x}$:

$$\mathbf{x} = \mathcal{T}(\mathbf{x}, D_{\boldsymbol{X}}, \mathcal{G}) + \mathbf{n}$$

To solve this fixed-point equation, we rely on the fact that $\mathcal{G}$ is a DAG, which enables to solve the fixed-point problem using the following simple iterative procedure. Starting with $\boldsymbol{z}_0 = \mathbf{n}$, we compute for $\ell = 1, \dots, d$ where $d$ is the number of nodes

$$\boldsymbol{z}_\ell = \mathcal{T}(\boldsymbol{z}_{\ell-1}, D_{\boldsymbol{X}}, \mathcal{G}) + \mathbf{n}$$

After $d$ iterations we obtain the following,

$$\boldsymbol{z}_d = \mathcal{T}(\boldsymbol{z}_d, D_{\boldsymbol{X}}, \mathcal{G}) + \mathbf{n}$$

Therefore, $\boldsymbol{z}_d$ is the solution of the fixed-point problem above, which corresponds to the observational sample associated to $\mathbf{n}$ according to our predicted SCM $z \to \mathcal{T}(z, D_{\boldsymbol{X}}, \mathcal{G})$.

**Interventional Prediction.** Recall that given a dataset $D_{\boldsymbol{X}}$ and its causal graph $\mathcal{G}$, $z \in \mathbb{R}^d \to \mathcal{T}(z, D_{\boldsymbol{X}}, \mathcal{G}) \in \mathbb{R}^d$ denotes the SCM infered by Cond-FiP. Let us also denote the coordinate-wise formulation of our SCM defined for any $z \in \mathbb{R}^d$ as $\mathcal{T}(z, D_{\boldsymbol{X}}, \mathcal{G}) = [[\mathcal{T}(z, D_{\boldsymbol{X}}, \mathcal{G})]_1, \dots, [\mathcal{T}(z, D_{\boldsymbol{X}}, \mathcal{G})]_d]$, where for all $i \in \{1, \dots, d\}$, $z \in \mathbb{R}^d \to [\mathcal{T}(z, D_{\boldsymbol{X}}, \mathcal{G})]_i \in \mathbb{R}$ is a real-valued function.

In order to intervene on this predicted SCM, we simply have to modify in place the predicted function. For example, assume that we want to perform the following intervention $\mathrm{do}(X_i) = a$. Then, to obtain the intervened SCM, we define a new function $z \to \mathcal{T}^{\mathrm{do}(X_i)=a}(z, D_{\boldsymbol{X}}, \mathcal{G})$ defined for any $z \in \mathbb{R}^d$ as: $[\mathcal{T}^{\mathrm{do}(X_i)=a}(z, D_{\boldsymbol{X}}, \mathcal{G})]_j := [\mathcal{T}(z, D_{\boldsymbol{X}}, \mathcal{G})]_j$ if $j \neq i$ and $[\mathcal{T}^{\mathrm{do}(X_i)=a}(z, D_{\boldsymbol{X}}, \mathcal{G})]_i := a$.

Now, using this intervened SCM $z \to \mathcal{T}^{\mathrm{do}(X_i)=a}(z, D_{\boldsymbol{X}}, \mathcal{G})$, we can apply the exact same generation procedure as the one introduced above to generate intervened samples according to our intervened SCM.

## E.3 Details on Encoder Training

We provide further details on training the encoder and show how recovering the noise is equivalent to learn the inverse causal generative process.

Recall that an SCM is an *implicit* generative model that, given a noise sample $\mathbf{N}$, generates the corresponding observation according to the following fixed-point equation in $\mathbf{X}$

$$\mathbf{X} = F(\mathbf{X}, \mathbf{N})$$

More precisely, to generate the associated observation, one must solve the above fixed-point equation in $\mathbf{X}$ given the noise $\mathbf{N}$. Let us now introduce the following notation that will be instrumental for the subsequent discussion: we denote $F_{\mathbf{N}}(z) : z \to F(z, \mathbf{N})$.

Due to the specific structure of $F$ (determined by the DAG $\mathcal{G}$ associated with the SCM), the fixed-point equation mentioned above can be efficiently solved by iteratively applying the function $F_{\mathbf{N}}$ to the noise (see Eq. (5) in the manuscript). As a direct consequence, the observation $\mathbf{X}$ can be expressed as a function of the noise:

$$\mathbf{X} = F_{\text{gen}}(\mathbf{N})$$

where $F_{\text{gen}}(\mathbf{N}) := (F_{\mathbf{N}})^{\circ d}(\mathbf{N})$, $d$ is the number of nodes, and $\circ$ denotes the composition operation. In the following we refer to $F_{\text{gen}}$ as the *explicit* generative model induced by the SCM.

Conversely, assuming that the mapping $z \to F_{\text{gen}}(z)$ is invertible, then one can express the noise as a function of the data:

$$\mathbf{N} = F_{\text{gen}}^{-1}(\mathbf{X})$$

Therefore, learning to recover the noise from observation is equivalent to learn the function $F_{\text{gen}}^{-1}$, which is exactly the inverse of the explicit generative model $F_{\text{gen}}$. It is also worth noting that under the ANM assumption (i.e. $F(\mathbf{X}, \mathbf{N}) = f(\mathbf{X}) + \mathbf{N}$), $F_{\text{gen}}$ is in fact always invertible and its inverse admits a simple expression which is

$$F_{\text{gen}}^{-1}(z) = z - f(z)$$

Therefore, in this specific case, learning the inverse generative model $F_{\text{gen}}^{-1}$ is exactly equivalent to learning the causal mechanism function $f$.